Contrib Mineral Petrol (2007) 154:335–356
DOI 10.1007/s00410-007-0196-6

ORIGINAL PAPER

Behaviour of zircon in high-grade metamorphic rocks: evidence from Hf isotopes, trace elements and textural studies

J. Sláma · J. Košler · R. B. Pedersen

Received: 11 August 2006 / Accepted: 7 March 2007 / Published online: 4 April 2007

Abstract Hf isotopic data of minerals in a mafic pyroxene granulite from the southern Bohemian Massif, together with their major and trace element composition and petrological observations were used to decipher the metamorphic history and behaviour of zircon in the granulite. The Hf isotopic composition in the minerals was used to estimate whether the decompression reaction, namely the consumption of garnet and rutile, could have provided Zr for the formation of newly grown metamorphic zircon. The age of the decompression reaction indicated by the evolution of Hf isotopes in garnet and orthopyroxene is between 333 and 331 Ma, i.e. ca. 7 Ma younger than the available U–Pb zircon ages from the Moldanubian granulites and than the newly obtained 343 ± 2 Ma laser ablation ICP-MS U–Pb age of zircons. The combination of bulk and in-situ Hf isotopic data, major and trace element composition and petrological modeling of P–T evolution revealed that the formation of zircons can not be related to the decompression phase of the evolution of the mafic granulites.

Keywords Hf isotopes · Zircon · Granulite · U–Pb dating · Laser ablation · ICP-MS · Garnet · Decompression · Metamorphic reaction

Communicated by T.L. Grove.

Electronic supplementary material The online version of this article (doi:10.1007/s00410-007-0196-6) contains supplementary material, which is available to authorized users.

J. Sláma (✉)
Department of Petrology and Structural Geology,
Charles University, Albertov 6,
128 43 Prague 2, Czech Republic
e-mail: slama@natur.cuni.cz

J. Sláma
Institute of Geology, Academy of Sciences of the Czech Republic, Rozvojová 135, 165 02 Prague 6, Czech Republic

J. Košler · R. B. Pedersen
Department of Earth Science, University of Bergen,
Allegaten 41, 5007 Bergen, Norway

Introduction

Isotopic dating of accessory minerals by means of U- and Th- decay is one of the most precise and accurate techniques for establishing the age of metamorphic rocks. There have been several attempts to link ages derived from accessory minerals, such as zircon or monazite, to specific metamorphic reactions, particularly in high-grade rocks, where several stages of accessory mineral growth and dissolution are common (e.g. Fraser et al. 1997; Pan 1997; Roberts and Finger 1997; Bingen et al. 2001; Degeling et al. 2001; Kelly and Harley 2005). Since the introduction of analytical techniques with spatial resolution capable of dating individual growth stages in accessory minerals, such as SHRIMP or LA ICP-MS (Andersen and Hinthorne 1972; Compston et al. 1984; Jackson et al. 1992, 1996; Hirata and Nesbitt 1995; Compston 1996; Williams 1998), it has become increasingly more important to link the obtained ages to specific mineral reactions and P–T conditions during metamorphism.

The isotopic ages of granulite facies metamorphism are often derived from U–Pb dating of mineral zircon ($ZrSiO_4$) and they are commonly interpreted as corresponding to the peak of granulite facies metamorphism (Pan 1997; Hoskin and Black 2000; Möller et al. 2002; Rubatto 2002; Tomaschek et al. 2003) or as representing

the age of the protolith of granulites (Kröner et al. 1988; Aftalion et al. 1989; Wendt et al. 1994; Vavra et al. 1996, 1999; Kröner et al. 2000; Andersen and Griffin 2004). Number of studies suggests that ages derived from metamorphic zircons or zircon overgrowths from high-grade rocks could represent other than the peak P–T conditions of metamorphic evolution. Zircon formation during the prograde metamorphic path (Schaltegger et al. 1999; Vavra et al. 1999; Bingen et al. 2001; Rubatto 2002; Hermann and Rubatto 2003; Bingen et al. 2004) or after the peak of metamorphism (Fraser et al. 1997; Roberts and Finger 1997; Vavra et al. 1999; Degeling et al. 2001; Hermann and Rubatto 2003; Whitehouse and Platt 2003) have previously been described as well as several zircon growth stages that reflect a complex polyphase metamorphic evolution (Schaltegger et al. 1999; Vavra et al. 1999; Bingen et al. 2001; Rubatto 2002; Hermann and Rubatto 2003; Kelly and Harley 2005). In metamorphic terranes that experienced fast burial and exhumation it is often difficult to define a single P–T metamorphic peak, since the highest temperatures often do not coincide with the highest pressures (e.g. Bingen et al. 2004).

In this study we have used trace element contents and Hf isotopic data from zircons and the coexisting metamorphic minerals to establish a link between metamorphic reactions that can potentially release Zr, Hf and other trace elements for the formation of zircons in the granulite facies rocks. Hafnium is a major chemical constituent in zircon and thus its isotopic composition can be determined in-situ by laser ablation (LA) ICP-MS technique (Thirlwall and Walder 1995; Griffin et al. 2000). It is also present in trace amount in other metamorphic minerals that, unlike zircon (Lu/Hf < 0.01), usually have a Lu/Hf ratio larger than 1. Due to its very low diffusivity (Cherniak et al. 1997; Koepke and Behrens 2001), Hf is thought to be immobile in metamorphic minerals even at pressures and temperatures reached at granulite facies conditions. Breakdown of metamorphic mineral phases is probably the only mechanism of Hf re-distribution in metamorphic rocks. As the ^{176}Hf in minerals is produced by beta decay of ^{176}Lu with a half-life of 37.17 Ga (Scherer et al. 2001), the ratio of radiogenic ^{176}Hf to the stable ^{177}Hf will vary for zircons and other metamorphic minerals subject to the mineral age and its Lu/Hf ratio. Because of the generally low Lu/Hf in zircon, its contrasting Hf isotopic composition can only arise by introduction of Hf with more radiogenic composition from other minerals. Accordingly, the ^{176}Hf/^{177}Hf in zircons that grew at different stages of metamorphism can be potentially used, together with the mass balance of other trace elements, such as REEs and Zr, as tracers of zircon-forming metamorphic reactions in high-grade rocks.

Overview of zircon-forming processes in metamorphic rocks

Several reaction mechanisms were previously described as potentially resulting in formation of zircon during high-grade metamorphism.

Growth of zircon during net-transfer reactions that release Zr requires Zr-rich phase(s), such as is garnet, amphibole, biotite or ilmenite, reacting to Zr-poor phase(s) with excess of ZrO_2 and SiO_2. Due to the low diffusivity of Zr, the growth of new zircon usually takes place near or within the reaction front (e.g. Fraser et al. 1997; Bingen et al. 2001, 2004; Degeling et al. 2001).

Growth of zircon from melt during partial melting (Roberts and Finger 1997) has been well documented in granulites by many authors (Schaltegger et al. 1999; Vavra et al. 1999; Rubatto 2002; Hermann and Rubatto 2003; Whitehouse and Platt 2003). Zircon crystallizes from the melt provided it is supersaturated by Zr. Zircon crystallization can take place either during the prograde-path (Schaltegger et al. 1999; Vavra et al. 1999; Rubatto 2002; Hermann and Rubatto 2003) or retrograde metamorphic conditions (Roberts and Finger 1997; Hermann and Rubatto 2003; Whitehouse and Platt 2003). Source of Zr for the newly-formed zircon is either from phases participating in the melt production, such as is biotite (Vavra et al. 1996), or Zr is released to the melt from older zircons dissolved during the stage of Zr-undersaturation in the melt (Roberts and Finger 1997).

The mechanism of *Ostwald ripening* has been suggested for the formation of metamorphic zircon overgrowths in granulites by Vavra et al. (1999). It requires the presence of Zr-supersaturated melt with respect to the larger zircon grains and Zr-undersaturated with respect to the smaller zircons. During the Ostwald ripening, the effect of surface energy minimization in the system causes that the small zircon grains can be readily dissolved in contact with melt droplets and Si and Zr are redistributed to the sites of new growth on larger zircon grains.

In-situ metamorphic crystal-chemical changes represent a widespread feature observed in zircon and can originate by diverse processes. *Solid-state recrystallization* of zircon at elevated P–T conditions (Schaltegger et al. 1999; Vavra et al. 1999; Hoskin and Black 2000; Möller et al. 2002; Bingen et al. 2004) reduces the crystal lattice strain, which is caused by unevenly distributed REEs and trace elements in the structure of zircon crystals. *Solid-state diffusion-reaction* process (Schaltegger et al. 1999; Vavra et al. 1999; Geisler et al. 2007) is induced by different α-decay doses between adjacent low-U-Th and high-U-Th domains in zircon crystal. It has been experimentally proven (Geisler et al. 2007) that re-equilibration (structural recovery) of such self-irradiated zircon proceeds in the presence of

aqueous fluid. *In-situ coupled dissolution-reprecipitation* processes affect zircons with very high contents of trace elements (Pan 1997; Tomaschek et al. 2003), which re-precipitate to trace element-poor zircon with REE-trace element-rich mineral inclusions (Geisler et al. 2007 and references therein). All these crystal-chemical changes are believed to proceed more readily in the presence of fluids (Schaltegger et al. 1999; Möller et al. 2002; Geisler et al. 2007) and are characterized by decrease of REEs and other trace elements concentrations. The U–Pb ages derived from structurally and chemically modified zircons are often difficult to interpret (Mezger and Krogstad 1997; Hoskin and Black 2000; Möller et al. 2002).

Collectively, the identification of a particular process that can lead to the formation of metamorphic zircons is limited by the fact that different processes can result in similar physical and chemical changes in zircon.

Geological setting and timing of metamorphism

The Blanský les granulite Massif is one of the major granulite bodies in southern part of the Bohemian Massif; it outcrops in an area of ca. 15 × 25 km NW of Český Krumlov (Fig. 1). The granulite represents part of the allochtonous Gföhl unit (Fuchs and Matura 1976; Matte et al. 1990; Fiala et al. 1995; Vrána et al. 1995; Franke 2000), which forms the uppermost tectonic member of the Moldanubian Zone, the core crystalline unit of the Variscan orogen in Europe (Dallmeyer et al. 1995). The Gföhl unit consists of felsic and mafic granulites, serpentinized garnet peridotites, pyroxenites and eclogites (Fuchs and Matura 1976; Franke 1989; Fiala et al. 1995). Migmatitic granitic gneisses (Gföhl gneisses) in the lower part of the Gföhl unit can represent overprinted felsic granulites (Fuchs and Matura 1976; Fiala et al. 1995). Structurally lower are the Varied (Drosendorf) unit composed of gneisses, orthogneisses, amphibolites, marbles, quartzites, calc-silicate and graphitic rocks, and the Monotonous (Ostrong) unit that consists of prevailing cordierite–biotite–sillimanite paragneisses, magmatic paragneisses and subordinate bodies of amphibolites, meta-eclogites and orthogneisses (Zoubek 1974; Matte et al. 1990; Fiala et al. 1995; O'Brien and Vrána 1995; Franke 2000). These two units have undergone amphibolite-facies metamorphism in the late stages of the Variscan orogeny.

The body of the Blanský les granulite contains mainly felsic garnet granulite gneisses (ca. 80%) with subordinate mafic pyroxene ± garnet granulites (ca. 10%), melanocratic biotite-garnet granulites (ca. 5%) and ultramafic rocks (ca. 5%), such as are serpentinized peridotites and eclogites (Fiala et al. 1987). All these rocks underwent HP-HT metamorphism during the Variscan orogeny with estimated peak conditions of 900–1,050°C and 1.5–2 GPa (Carswell and O'Brien 1993; Kotková and Harley 1997; O'Brien and Rötzler 2003). Following the peak of metamorphism, there was almost isothermal decompression to mid-crustal level pressures with an overprint at 800–900°C and 0.8–1.2 GPa (Cooke 2000) and subsequent near-isobaric cooling. The retrogression of granulites is documented by garnet breakdown and formation of secondary-corona structures, change of garnet to biotite and kyanite to sillimanite (Owen and Dostal 1996; O'Brien and Rötzler 2003).

The age of metamorphism is constrained by a number of U–Pb zircon ages at ca. 340 Ma (van Breemen et al. 1982; Kröner et al. 1988, 2000; Aftalion et al. 1989; Wendt et al. 1994; Friedl et al. 2003; Kotková et al. 2003). This age has often been interpreted as corresponding to the time of granulite HP-HT metamorphic peak, but Roberts and

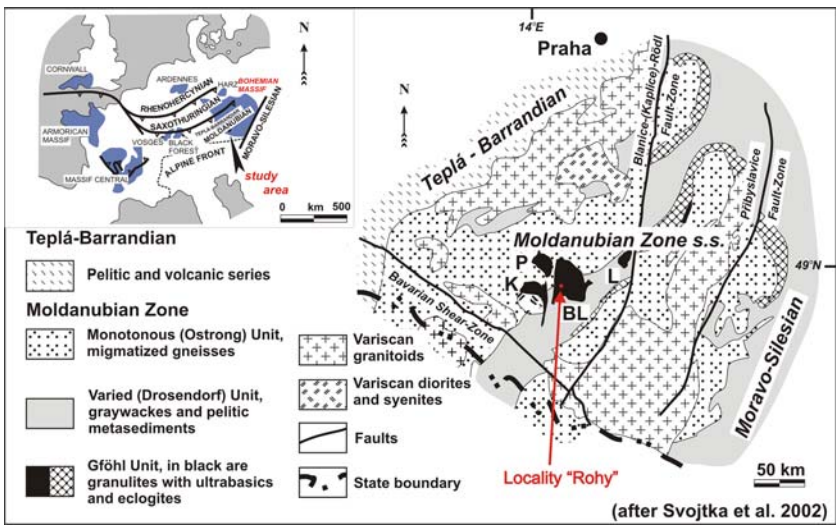

Fig. 1 Schematic map of the Bohemian Massif showing position of the Blanský les granulite and the studied locality

Finger (1997) argue for zircon crystallization from partial melt during the retrograde P–T path, and Kröner et al. (2000) and Janoušek et al. (2004) propose that zircons that grew under granulite peak conditions and subsequent rapid decompression are similar in age. Some zircon cores from granulites of the Blanský les gave a U–Pb age of ca. 470 Ma (Kröner et al. 2000), coincident with a whole-rock Rb–Sr age obtained by Janoušek et al. (2004) who interpreted it as corresponding to the age of the granulite protolith.

Methods

Samples of the mafic granulite were collected from natural outcrops at locality Rohy (N 48°53′55″, E 14°14′27″) in the SW part of the Blanský les granulite massif, ca. 6 km NE of Chvalšiny (Fig. 1). Polished sections (~100 μm thick) were prepared for petrographical, electron microprobe and laser ablation ICP-MS study, the rest of the sample material was crushed for mineral separation and milled for chemical analyses. Minerals were separated using sieving, conventional heavy liquid techniques and magnetic separation. Zircons were mounted in 1-inch epoxy resin blocks and polished to obtain flat surfaces suitable for electron microbeam and laser ablation analyses.

Whole rock major and trace element composition was measured using ICP-OES (Masaryk University, Brno) and ICP-MS (University of Bergen) techniques. Zircon backscattered electron (BSE) imaging and major element spot analyses of minerals were carried out using a CamScan S4 and CamScan CS3200 electron microscopes at Charles University and Czech Geological Survey in Prague and Cameca SX-100 electron microprobe at Masaryk University in Brno. Perple_X software by James Connolly (IMP-ETH Zurich) was used to calculate P–T pseudosection for the studied mafic granulite.

U–Pb dating of polished zircon grains was carried out using a New Wave UP-213 laser attached to a single collector Finnigan Element 2 ICP-MS at the University of Bergen. Laser was fired at repetition rate of 10 Hz and energy of 3 J/cm^2. Linear laser rasters (50 or 100 microns) were produced by repeated scanning of the leaser beam at a speed of 10 microns/s across the zircon sample surface. The technique closely followed the procedure described in Košler et al. (2002). The signal was collected for 35 s (gas blank) followed by 180 s of laser ablation signal. Raw data were corrected for dead time of the electron multiplier and processed off line in a spreadsheet-based program (Lamdate—Košler et al. 2002) and plotted on concordia diagrams using Isoplot (Ludwig 2003). Data reduction included correction for gas blank, laser-induced elemental fractionation of Pb and U and instrument mass bias. Minor formation of oxides of U and Np was corrected for by adding signal intensities at masses 249, 253 and 254 to the intensities at masses 233, 237 and 238, respectively. No common Pb correction was applied to the data. Details of data reduction and corrections are described in Košler et al. (2002) and Košler and Sylvester (2003). Zircon reference material 91500 (1,065 Ma—Wiedenbeck et al. 1995) was periodically analysed during this study.

Trace element and REE concentrations in zircon and other minerals were measured in thin sections using the same laser ablation ICP-MS setup. The laser was fired at repetition rate of 10 Hz, using 5 J/cm^2 laser energy and spot size of 60 microns. Synthetic silicate glass NIST-612 was used to calibrate the trace element concentration data, repeat measurements of NIST-610 and BCR-2 glasses were carried out for quality control purposes. Data for gas blank were acquired for 60 s followed by 80 s of laser ablation signal. Time-resolved signal data were processed using the GLITTER software; caution was taken to constrain the signal to chemically homogeneous parts of the crystals and to avoid any inclusions and inhomogenities that can be potentially present in the analysed minerals.

Measurement of Hf isotopes in mineral separates (except for zircon) was carried out after an ion exchange chromatographic separation that followed the procedure described in Munker et al. (2001). The faraday cup configuration of Finnigan Neptune multicollector (MC) ICP-MS at the University of Bergen was set as follows: L4—^{172}Yb, L3—^{173}Yb, L2—^{175}Lu, L1—^{176}Hf, C—^{177}Hf, H1—^{178}Hf, H2—^{179}Hf, H3—^{180}Hf, H4—^{182}W. Samples were aspirated to the ICP in 2% HNO_3 using solution uptake rate of 50 μl/min and APEX (Elemental Scientific) desolvating nebulizer. The instrument sensitivity was 40 V/ppm of Hf measured at mass 180. The data acquisition procedure consisted of 90 integration cycles acquired over a period of 6 min, followed by 5 min of washout with a mixture of 2% HNO_3–0.2 N HF composition. ^{179}Hf/^{177}Hf = 0.7325 (Patchett and Tatsumoto 1980) value and the exponential law were used for mass bias correction of calculated ratios. Measurement of the Hf isotopic composition in reference solution of JMC475 over the period of this study gave a mean ^{176}Hf/^{177}Hf value of 0.282158 ± 0.000022 (2 SD). The Lu/Hf ratios used for age correction of Hf isotopic ratios were measured in a solution aliquot taken before the Hf separation. A Finnigan Element 2 ICP-MS at the University of Bergen was used for Lu/Hf ratio measurements and the obtained values were verified by subsequent laser ablation ICP-MS analyses of individual minerals. λ^{176}Lu decay constant of 1.865 × 10^{-11} (Scherer et al. 2001), CHUR values of ^{176}Hf/^{177}Hf = 0.282772, ^{176}Lu/^{177}Hf = 0.0332 (Blichert-Toft and Albarède 1997) and t = 343 Ma obtained from LA ICP-MS analysis of zircons were used to calculate the

initial εHf values. Hf isotopic analyses of minerals in this study represent single measurements that consists of 90 integrations, each 4 s long.

Measurement of Hf isotopes in zircons in thin sections was carried out using the New Wave UP-213 laser attached to the Finnigan Neptune multicollector ICP-MS. The laser was fired with energy of 2.8 J/cm^2, laser beam diameter of 20–80 microns and repetition rate of 10 Hz. Laser beam was scanned across the zircon surface to ablate a linear raster 50 or 100 microns long. Data for gas blank were acquired for 50 s followed by 210 s of laser ablation. The typical signal intensity was 0.6 V for ^{180}Hf. Data were corrected for gas blank. Value of ^{179}Hf/^{177}Hf = 0.7325 (Patchett and Tatsumoto 1980) and the exponential law were used for mass bias correction of interfering elements and Hf isotopes. Interferences of Lu and Yb on ^{176}Hf were corrected for by measuring the intensity of the interference-free ^{175}Lu and ^{173}Yb isotopes and using the recommended values of ^{176}Lu/^{175}Lu = 0.02669 (DeBièvre and Taylor 1993) and ^{176}Yb/^{173}Yb = 0.7952 (Lapen et al. 2004), respectively, to calculate ^{176}Lu/^{177}Hf.

Zircon 91500 reference sample (Wiedenbeck et al. 1995) was periodically analyzed during this study and gave a mean ^{176}Hf/^{177}Hf value of 0.282293 ± 0.000036 (2 SD). λ^{176}Lu decay constant of 1.865×10^{-11} (Scherer et al. 2001), CHUR values of ^{176}Hf/^{177}Hf = 0.282772 and ^{176}Lu/^{177}Hf = 0.0332 (Blichert-Toft and Albarède 1997) and t = 343 Ma obtained from LA ICP-MS analysis of zircons were used to calculate the initial εHf values.

Petrography and major element composition of minerals

The studied mafic garnet-pyroxene granulite is exposed as a boudin several tens of meters in size that is surrounded by felsic granulites. It consists of clinopyroxene, orthopyroxene, garnet, plagioclase, K-feldspar, quartz, amphibole and biotite and accessory ilmenite, rutile, apatite, magnetite, zircon and baddeleyite.

Clinopyroxene is of diopside composition (X_{Wo} = 0.46, X_{En} = 0.38, X_{Fs} = 0.16) and it represents a major phase (ca. 27 wt%) in the granulite. It forms anhedral grains several hundreds of microns in size. Larger grains of clinopyroxene porphyroblasts with exsolutions of orthopyroxene are also present in the matrix.

Garnet (ca. 20 wt% in the rock) occurs as up to 2 mm large, oval grains (Fig. 2) with zonality in major elements showing a prograde increase of Mg from the core (X_{Alm} = 0.37, X_{Grs} = 0.34, X_{Prp} = 0.28, X_{Sps} = 0.01, X_{Mg} = 0.303) towards the rim (X_{Alm} = 0.36, X_{Grs} = 0.33, X_{Prp} = 0.30, X_{Sps} = 0.01, X_{Mg} = 0.319) and a retrograde outer rim, with increased content of Fe (X_{Alm} = 0.53, X_{Grs} = 0.22, X_{Prp} = 0.21, X_{Sps} = 0.04, X_{Mg} = 0.185; Fig. 3). The garnet rims are in most cases replaced by reaction corona that formed as a result of decompression (Thost et al. 1991; Owen and Dostal 1996). The corona consists of two concentric zones: the symplectitic assemblage of orthopyroxene, anorthite and magnetite (zone I in Fig. 2d) formed immediately adjacent to the garnet and the quartz-absent plagioclase (An_{50})-orthopyroxene corona with scarce amphibole grains (zone II in Fig. 2d) further away from the garnet. The extent of garnet consumption varies subject to its size; the largest grains are replaced by up to 50% by the reaction products, the smaller garnet grains are often completely replaced by the reaction corona assemblage. Inclusions in garnet are common and usually formed by rutile, apatite, quartz, plagioclase and zircon.

Feldspar (ca. 31 wt% of the granulite) is represented by antiperthite, anorthite and andesine. The antiperthitic feldspar in the matrix and in inclusions in the garnet represents a texturally older assemblage that is characterised by K-feldspar (X_{Kfs} = 0.9, X_{Ab} = 0.09, X_{An} = 0.01) exsolutions in the plagioclase of andesine composition (X_{Ab} = 0.65, X_{An} = 0.3, X_{Kfs} = 0.05); only rarely is the andesine free of K-feldspar lamellae. The anorthite (X_{An} = 0.92, X_{Ab} = 0.08) is only present in the fine-grained symplectitic coronas around garnet as a product of garnet decompression decay (zone I, Fig. 2d). The plagioclase (X_{An} = 0.5, X_{Ab} = 0.5) occurs in zone II of the garnet corona and it probably formed by recrystallization of the andesine originally present in the matrix by addition of Ca from the reacting garnet.

Orthopyroxene (ca. 5 wt% of the rock) occurs as a product of garnet decay in both zones of the reaction corona together with plagioclase (Fig. 2). It has a uniform hypersthene composition (X_{En} = 0.65).

Quartz (ca. 11 wt% of the rock) occurs as anhedral grains in the matrix. Small amount of quartz was probably consumed in the corona forming reaction around garnet.

Amphibole is represented by common magnesio-hornblende. It forms euhedral to anhedral grains up to several hundreds microns in size in the quartz-free, plagioclase corona in the reaction zone II (Fig. 2c). Its abundance in the rock is variable with ca. 3 wt% in domains with almost no biotite that probably represent the least retrogressed parts of the rock.

Biotite occurs as ca. 1 mm elongate grains in the matrix and often also as a product of garnet retrogression. Its abundance is variable (up to 10 wt%) subject to the extent of granulite retrogression.

Ilmenite (ca. 1 wt% of the rock) occurs as anhedral grains up to 1 mm in size in the matrix assemblage. Smaller, anhedral or oval grains occur in the matrix as well as within the reaction corona around garnet and morphologically resemble the rutile grains.

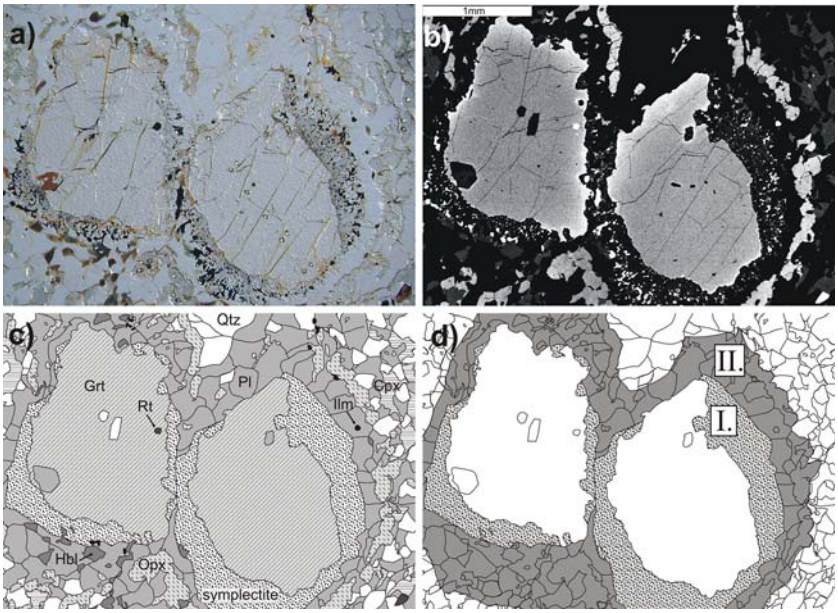

Fig. 2 Decompression reaction corona around garnet. **a** Optical image in transmitted polarized light; **b** corresponding BSE image; **c** sketch of mineral distribution in the reaction corona; **d** reaction zones: *I.* symplectitic assemblage of Opx, An and Mag, *II.* Qtz–depleted corona of An, Opx and Hbl

Rutile forms ca. 0.15 wt% of the rock and it occurs as anhedral grains in the matrix and ovoid- and needle-shaped inclusions in the garnets (Fig. 2c). Rutile has been partly changed to ilmenite during the metamorphic evolution of the mafic granulite.

Magnetite occurs as small anhedral grains seldom larger than 20 microns in the symplectitic assemblage in coronas surrounding the garnet (zone I, Fig. 2).

Zircon is present in the studied granulite as up to 500 microns large grains with ovoid and soccer-ball shapes; it is rarely prismatic and the surface of the grains is often pitted suggesting zircon alteration. It occurs in the matrix, in the reaction corona around garnet and as inclusions in the garnet and plagioclase. The BSE imaging revealed at least two zircon populations present as (1) bright-BSE, often U-rich domains, with unclear irregular zoning, and as (2) dark-BSE domains that locally contain ghost or fading zoning. Dark-BSE zircon rimming the bright-BSE zircon is often radially cracked due to alteration-induced volume changes. Small zircon grains (up to 10 microns) are sometimes associated with larger (~1 mm) ilmenite crystals in the matrix; they rim the ilmenite grains or occur in the cracks inside the ilmenite.

Baddeleyite occurs as up to 100 microns large euhedral crystals, exclusively within or at the margins of small ilmenite grains where the surrounding mineral is plagioclase or pyroxene.

Trace element composition of minerals

Concentration of Zr in metamorphic minerals is important particularly with respect to its potential release during metamorphic reactions and the availability to form metamorphic zircon (see also Fraser et al. 1997; Bingen et al. 2001; Degeling et al. 2001). Most of Zr in the granulite is bound in accessory zircon and rutile (average Zr content of 2,914 ppm, Fig. 4). Amphibole with the average concentration of 211 ppm Zr is also a significant Zr repository (see Fraser et al. 1997). Zr content in amphibole varies subject to the spatial distribution of amphibole grains in the rock; amphiboles adjacent to the reaction rims around garnet have higher concentration of Zr (calculated average concentration from 11 analyses is 237 ppm, Table 1), whereas amphibole grains in the matrix away from the garnet have Zr content of 165 ppm (average of six analyses, Table 1). Concentrations of Hf, Th, U and Y in amphibole grains in the corona and in the matrix follow a similar pattern.

Distribution of trace elements in biotite varies subject to its textural (spatial) relations with other minerals in the granulite. Larger biotite crystals in the matrix and biotite around the reaction coronas in garnets have somewhat higher contents of Hf and Zr and lower contents of Y in comparison to the biotite formed by garnet retrogression (cf. Table 1). In addition, the biotite grains in the matrix and adjacent to the garnet corona that are spatially associated with ilmenite have lower contents of Zr and Hf and higher content of Y compared to the biotite grains that are not in contact with ilmenite.

The two populations of ilmenite present in the studied mafic granulite have slightly different trace element compositions. The larger ilmenite grains in the matrix have lower concentrations of Zr (35–44 ppm Table 2) and Hf (1.7–3.7 ppm, Table 2). The population of smaller ilmenite grains has generally higher concentration of trace elements,

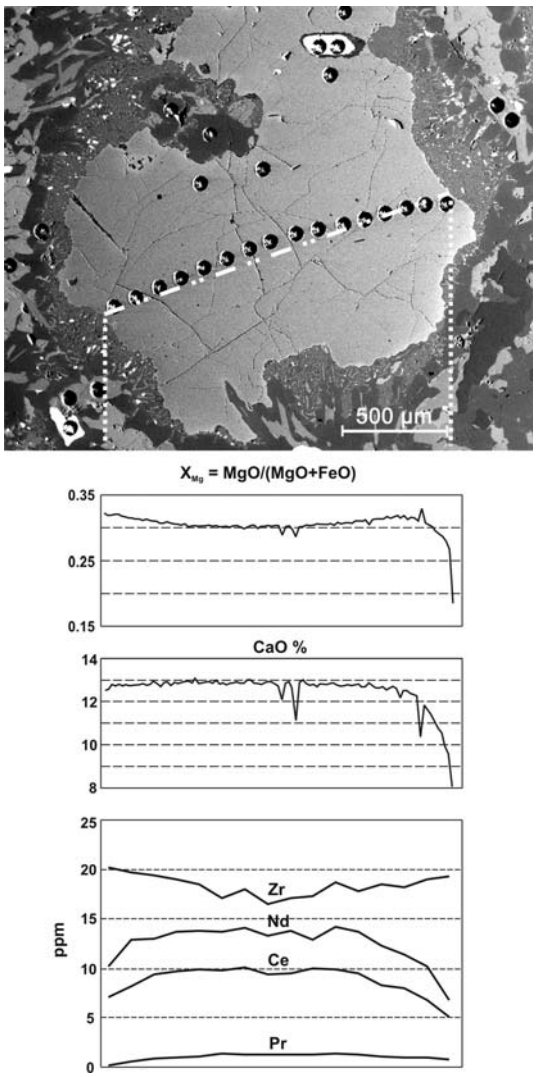

Fig. 3 Major (electron microprobe data) and trace (laser ablation ICP–MS data) element zoning in garnet from the mafic granulite. For a complete set of major and trace elements data, see ESM_Table 2 in the electronic supplementary material (analyses are marked as profile 1)

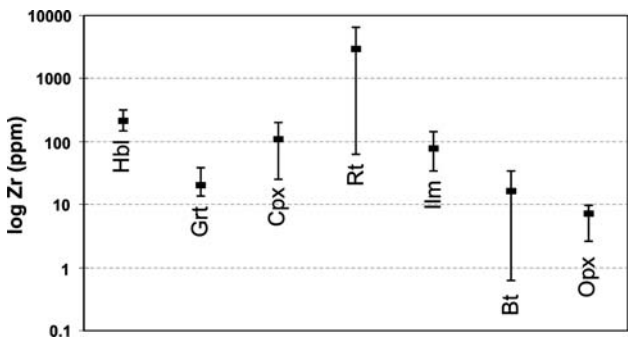

Fig. 4 Range of Zr contents in minerals from the studied mafic granulite

including Zr (~97 ppm) and Hf (~10 ppm; eight analyses—Table 2). The shape of smaller ilmenite grains and the relics of rutile within these ilmenites suggest that they formed from the rutile. The large range of Zr and Hf concentrations in these ilmenites is likely to be related to the variations in trace elements concentrations in the primary rutile from which the ilmenite formed. A possible significance of ilmenite as a donor of Zr to the newly formed zircon has been proposed by Bingen et al. (2001).

The Zr content in rutile is highly variable even within individual grains but is generally lower in the ovoid-shaped rutile grains enclosed in the garnet (Zr content of 63–1,485 ppm, Table 2) compared to the anhedral rutiles present in the matrix (average Zr content of 4,084 ppm, five analyses, Table 2).

Garnet, clinopyroxene, orthopyroxene, plagioclase and apatite have uniform trace element composition, as reported in Tables 1 and 2. Laser ablation ICP-MS analyses of large garnet grains allowed studying the trace elements distribution within the individual grains. A linear profile with 16 laser spot analyses within one garnet grain revealed a weak zoning in the Zr content which increases from the garnet core to the rim (Fig. 3). Similar pattern was observed also in other garnet grains in the studied granulite.

The concentrations of REE in all studied minerals were normalized to chondrite REE values (Sun and McDonough, 1989) and plotted as spider diagrams in Fig. 5. Garnets have a uniform REE composition (Fig. 5a), which is characterised by enrichment of HREE relative to LREE (La_N/Yb_N ~ 0.02), typical weak negative Eu anomaly (Eu/Eu* = 0.47–0.88, average 0.72) and a positive Ce anomaly (Ce/Ce* = 0.92–14, average 6.9). Ce, Pr and Nd contents decrease gradually from the core to the garnet rim (Fig. 3). Two distinctly different REE patterns and variable HREE distribution were found in the studied amphiboles. Similar to other trace elements, the contents of REE are higher in amphiboles that occur close to the garnet reaction rims compared to the amphiboles in the matrix (Fig. 5b). Amphiboles that are spatially associated with garnet corona have flat REE patterns with slight enrichment of LREE relative to HREE (La_N/Yb_N = 0.71–2.4, average 1.4; Table 1) and a negative Eu anomaly (Eu/Eu* = 0.23–0.35, average 0.29; Table 1). The amphibole grains in the matrix have much steeper REE pattern (La_N/Yb_N = 5.1–5.8, average 5.3; Table 1) and a less expressed Eu anomaly (Eu/Eu* = 0.23–0.61, average 0.47; Table 1). The REE distribution in clinopyroxene (Fig. 5c) has typically weak LREE enrichment relative to HREE (La_N/Yb_N = 0.93–3.36, average 1.8; Table 1) and a strong negative Eu anomaly (Eu/Eu* = 0.13–0.41, average 0.30; Table 1). Orthopyroxene has lower contents of REE and its REE pattern shows an enrichment of HREE relative to

Table 1 Average (in bold) trace element and REE concentrations in major minerals from the mafic granulite

Mineral	Amphibole		Orthopyroxene	Garnet	Clinopyroxene	Biotite		
*Comment	Matrix (n = 6)	Corona (n = 11)	(n = 14)	(n = 49)	(n = 14)	Corona (n = 10)	Near ilmenite in corona (n = 6)	Residue after garnet decay (n = 2)
Y	**56** (46–72.9)	**228** (172–315)	**11** (0.3–23)	**81** (66–161)	**40** (23–67)	**2.2** (0.5–5.2)	**6.5** (0.5–21)	~12
Zr	**165** (147–188)	**237** (205–313)	**7.3** (2.6–9.6)	**20** (14–39)	**109** (25–204)	**23** (16–33)	**10** (6.5–16)	~1.0
Hf	**5.1** (4–6.3)	**7.6** (4.8–11)	**0.3** (0.1–0.4)	**0.3** (0.1–0.8)	**4.3** (1.0–7.8)	**0.9** (0.5–1.2)	**0.6** (0.4–0.87)	~0.1
Th	**1.3** (1.1–1.6)	**1.9** (1.6–2.5)	**0.2** (0.01–0.5)	**0.1** (0.003–2.7)	**0.5** (0.1–1.3)	**0.1** (0.002–0.2)	<0.1	~0.1
U	**0.1** (0.1–0.2)	**0.3** (0.2–0.4)	**0.02** (0.001–0.1)	**0.1** (0.01–0.4)	**0.1** (0.01–0.7)	<0.1	<0.1	~0.01
La	**41** (37–50)	**37** (31–46)	**0.7** (0.1–5.1)	**0.2** (0.02–5.3)	**5.7** (0.4–11)	**0.8** (0.04–1.7)	**1.2** (0.4–3.0)	~1.4
Ce	**143** (120–187)	**150** (125–198)	**1.0** (0.2–7.5)	**7.6** (3.1–12)	**36** (1.6–60)	**1.4** (0.2–2.7)	**2.2** (0.5–6.5)	~3.0
Pr	**27** (23–36)	**27** (23–35)	**0.2** (0.03–1.2)	**0.9** (0.2–1.9)	**6.4** (0.3–11)	**0.2** (0.01–0.4)	**0.4** (0.1–1.2)	~0.5
Nd	**122** (98–164)	**136** (110–185)	**0.7** (0.2–4.3)	**10** (4.4–14)	**35** (1.6–58)	**0.9** (0.2–1.4)	**1.8** (0.2–6.0)	~2.5
Sm	**23** (18–32)	**38** (29–54)	**0.7** (0.4–0.9)	**7.0** (5.1–8.6)	**10** (0.4–16)	**0.4** (0.2–0.7)	**0.8** (0.04–2.6)	~1.1
Eu	**2.9** (2.6–3.5)	**3.9** (3.4–4.7)	**0.3** (0.03–1.6)	**2.0** (1.6–2.4)	**0.8** (0.03–1.6)	**0.3** (0.1–0.4)	**0.2** (0.1–0.4)	~0.3
Gd	**16** (12–23)	**44** (35–58)	**0.8** (0.3–1.6)	**11** (8.6–18)	**8.7** (0.3–17)	**0.5** (0.2–1.0)	**1.2** (0.3–3.1)	~1.7
Tb	**2.0** (1.5–2.7)	**6.9** (5.2–9.2)	**0.2** (0.1–0.4)	**2.0** (1.6–3.3)	**1.2** (0.04–2.6)	**0.1** (0.01–0.2)	**0.2** (0.01–0.6)	~0.3
Dy	**11** (9.1–16)	**45** (36–58)	**1.7** (0.1–3.2)	**14** (12–26)	**6.9** (0.2–14)	**0.4** (0.02–1.1)	**1.3** (0.04–4.7)	~2.0
Ho	**2.1** (1.6–2.7)	**9.0** (6.9–12)	**0.4** (0.01–0.9)	**3.0** (2.4–5.1)	**1.3** (0.04–2.7)	**0.1** (0.01–0.2)	**0.3** (0.01–0.9)	~0.4
Er	**5.4** (4.5–6.9)	**24** (19–35)	**1.4** (0.04–2.9)	**8.9** (7.0–15)	**3.3** (0.1–6.3)	**0.2** (0.03–0.6)	**0.8** (0.1–2.7)	~1.2
Tm	**0.8** (0.6–0.9)	**3.3** (2.1–5.3)	**0.3** (0.1–0.6)	**1.4** (1.0–2.3)	**0.4** (0.01–0.7)	<0.1	**0.1** (0.005–0.4)	~0.2
Yb	**5.2** (4.7–5.9)	**20** (11–35)	**1.9** (0.04–3.6)	**10** (7.6–17)	**2.7** (0.1–4.7)	**0.2** (0.04–0.8)	**0.8** (0.1–2.5)	~1.1
Lu	**0.7** (0.6–0.8)	**2.8** (1.3–5.6)	**0.3** (0.2–0.6)	**1.4** (1.0–2.3)	**0.4** (0.01–0.6)	<0.1	**0.1** (0.01–0.1)	~0.2
Eu/Eu*	**0.47** (0.23–0.61)	**0.29** (0.23–0.35)	**0.25** (0.07–0.58)	**0.72** (0.47–0.88)	**0.30** (0.13–0.41)	**2.2** (0.2–3.5)	**1.5** (0.4–3.7)	~0.6
Ce/Ce*	**1** (0.96–1.08)	**1.1** (1–1.2)	**1** (0.4–2.2)	**6.9** (0.92–14)	**1.3** (0.5–1.8)	~0.6	~0.7	~0.9
La_N/Yb_N	**5.3** (5.1–5.8)	**1.4** (0.71–2.4)	**0.12** (0.01–0.67)	**0.02** (0.002–0.4)	**1.8** (0.93–3.36)	**1.4** (0.6–3.3)	**1.9** (0.8–4.2)	~0.8

Values are concentrations in ppm, range of concentrations is given in the brackets. *comment: position in the rock (n number of analyses). $Eu/Eu^* = Eu_N/\sqrt{(Sm_N*Gd_N)}$, $Ce/Ce^* = Ce_N/\sqrt{(La_N*Pr_N)}$, normalisation to C1 after Sun and McDonough (1989). Complete set of electron microprobe and laser ablation ICP–MS analyses is available from the journal's electronic supplementary material (ESM_Tables 1–3, 5, 6)

Table 2 Average (in bold) trace element and REE concentrations in accessory minerals from the mafic granulite

Mineral	Zircon			Apatite	Rutile		Ilmenite	
*Comment	Bright in BSE (n = 5)	Ghost zoned in BSE (n = 4)	Dark in BSE (n = 18)	(n = 5)	Garnet (n = 3)	Matrix (n = 5)	Larger grains in matrix (n = 3)	Smaller grains in matrix and garnet (n = 8)
Y	**2,300** (1,325–3,670)	**630** (179–1,121)	**60** (36–87)	**254** (4.5–617)	**1.5** (1.3–1.7)	**1.8** (1.0–2.3)	**1.1** (0.7–1.4)	**1** (0.6–2.7)
Zr	N/A	N/A	N/A	[a]	**965** (63–1,485)	**4,084** (2,408–6,569)	**40** (35–44)	**97** (55–151)
Hf	**13,570** (12,240–17,990)	**14,080** (10,500–19,164)	**13,075** (7,230–19,783)	[a]	**40** (8.6–72)	**104** (57–160)	**2.3** (1.7–3.7)	**10** (5.4–15)
Th	**1,370** (937–2,035)	**571** (79–1,375)	**75** (34–153)	**44** (26–54)	<0.1	**0.3** (0.1–0.7)	<0.1	**0.3** (0–1.8)
U	**1,130** (838–1,346)	**1,016** (447–1,806)	**454** (158–1,145)	**23** (0.9–39)	**8.2** (0.03–13)	**122** (111–135)	**0.3** (0–0.6)	**0.55** (0–4.3)
Th/U	**1.22** (0.73–1.65)	**0.5** (0.18–0.76)	**0.20** (0.10–0.54)	N/A	N/A	N/A	N/A	N/A
La	**0.5** (0.2–0.8)	**0.4** (0.02–0.8)	**0.2** (0.02–1.1)	**731** (135–986)	[a]	[a]	[a]	[a]
Ce	**7.8** (3.4–15)	**7** (2.5–13)	**5** (1.3–8.2)	**1,579** (137–2,341)	[a]	[a]	[a]	[a]
Pr	**0.2** (0.1–0.3)	**0.4** (0.09–0.7)	**0.2** (0.09–0.4)	**294** (34–450)	[a]	[a]	[a]	[a]
Nd	**8** (1.2–20)	**6.8** (5.2–11)	**6** (1.3–9)	**1,194** (76–1,666)	[a]	[a]	[a]	[a]
Sm	**7.7** (2.8–13)	**4.5** (2.0–6.1)	**3.5** (1.4–5.4)	**202** (179–267)	[a]	[a]	[a]	[a]
Eu	**1.8** (1.1–2.8)	**1.4** (0.4–3.0)	**0.7** (0.3–1.1)	**12** (8.0–17)	[a]	[a]	[a]	[a]
Gd	**22** (12–37)	**7.4** (1.0–20)	**2.1** (0.8–5.6)	**115** (16–203)	[a]	[a]	[a]	[a]
Tb	**14** (6.7–23)	**4.6** (1.5–7.2)	**1** (0.4–1.5)	**14** (9.3–23)	[a]	[a]	[a]	[a]
Dy	**192** (92–312)	**53** (15–95)	**8** (4.6–12)	**66** (40–130)	[a]	[a]	[a]	[a]
Ho	**76** (41–121)	**20** (6–37)	**1.8** (1.1–2.9)	**9.4** (1.0–22)	[a]	[a]	[a]	[a]
Er	**349** (214–509)	**90** (23–163)	**6.2** (3.2–10)	**27** (16–55)	[a]	[a]	[a]	[a]
Tm	**87** (56–126)	**22** (5.9–40)	**1.3** (0.7–2.4)	**3.0** (1.6–6.4)	[a]	[a]	[a]	[a]
Yb	**927** (594–1,298)	**243** (59–427)	**12** (5.1–29)	**16** (8.5–36)	[a]	[a]	[a]	[a]
Lu	**142** (117–173)	**35** (8.8–56)	**1.6** (0.7–5.1)	**2.0** (1.1–4.4)	[a]	[a]	[a]	[a]
Eu/Eu*	**0.46** (0.35–0.57)	~0.82	**0.97** (0.58–1.18)	**0.2** (0.18–0.22)	N/A	N/A	N/A	N/A
Ce/Ce*	**13** (3.7–21)	~6.4	**7.7** (4–12)	~0.8	N/A	N/A	N/A	N/A
La_N/Yb_N	**0.0004** (0.0001–0.0007)	~0.001	**0.01** (0.003–0.013)	**44** (19–64)	N/A	N/A	N/A	N/A
Lu_N/Sm_N	**196** (123–239)	**65** (35–123)	**5.3** (1.8–14)	N/A	N/A	N/A	N/A	N/A

Values are concentrations in ppm, range of concentrations is given in the brackets. *comment: position in the rock (n—number of analyses). N/A = data not available. $Eu/Eu^* = Eu_N/\sqrt{(Sm_N*Gd_N)}$, $Ce/Ce^* = Ce_N/\sqrt{(La_N*Pr_N)}$, normalisation to C1 after Sun and McDonough (1989). Complete set of laser ablation ICP–MS analyses is available from the journal's electronic supplementary material (Tables 7–10)

[a] Analysis below limit of detection

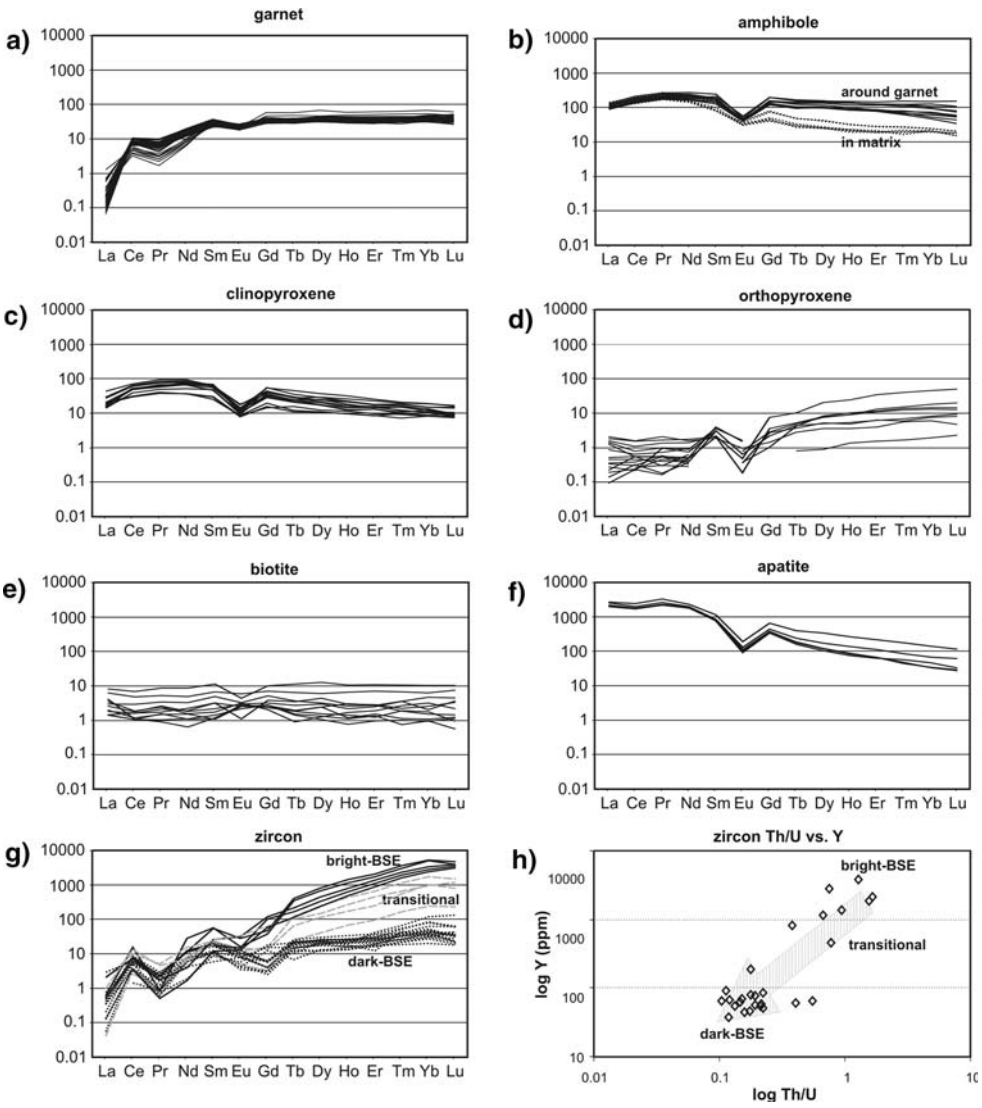

Fig. 5 **a–g** REE chondrite normalized spider plots of minerals from the mafic granulite. Data were normalized using C1 values of Sun and McDonough (1989); **h** Th/U versus Y plot of analysed zircons (cf. Fig. 6 and Plates 1–4 in the electronic supplementary material for textural relations). For a complete set of REE data, see ESM_Tables 1–3, 5, 6, 9, 10 in the electronic supplementary material

LREE (La_N/Yb_N = 0.01–0.67, average 0.12; Table 1, Fig. 5d) and a significant negative Eu anomaly (Eu/Eu* = 0.07–0.58, average 0.25; Table 1). Biotite has also very low REE concentrations that vary between ca. 1 and 10 times the chondritic contents. The REE pattern for biotite is flat (La_N/Yb_N ~ 2; Table 1, Fig. 5e) and there is no distinct Eu anomaly.

The studied apatite is rich in REEs (~3,000× enriched in LREE relative to chondrite) and it has a distinct steep REE normalized pattern with enrichment of LREE relative to HREE (La_N/Yb_N ~ 44; Table 2) and a significant negative Eu anomaly (Eu/Eu* ~ 0.2; Table 2, Fig. 5f). The REE concentrations in rutile and ilmenite are close to the detection limits of the LA ICP-MS and the data could not be reliably interpreted.

The trace element and REE composition of zircon, which is often interpreted as reflecting the zircon origin (Williams et al. 1996; Schaltegger et al. 1999; Vavra et al. 1999; Möller et al. 2002; Rubatto 2002; Hermann and Rubatto 2003; Kelly and Harley 2005) is reported in Table 2 and plotted in Fig. 5g, h and Fig. 6 (see also Plates 1–4 in the electronic supplementary material). The two zircon populations that can be discriminated on the basis of BSE imaging have also different trace element compositions. Relatively high Th/U ratios together with higher contents of Y, Th and U in bright-BSE zircon domains contrast to lower Y, Th, U and Th/U ratios in dark-BSE zircon domains. In addition, the REE patterns of the bright-BSE zircon domains (Fig. 5g; Zrn 4 and 5 in Fig. 6) show typical ''magmatic'' features with steep normalized pattern enriched in HREE relative to LREE (La_N/Yb_N ~ 0.0004; Lu_N/Sm_N ~ 196; Table 2), a negative Eu anomaly (Eu/Eu* ~ 0.46; Table 2) and a positive Ce anomaly (Ce/Ce* ~ 13; Table 2). The dark-BSE areas of zircons

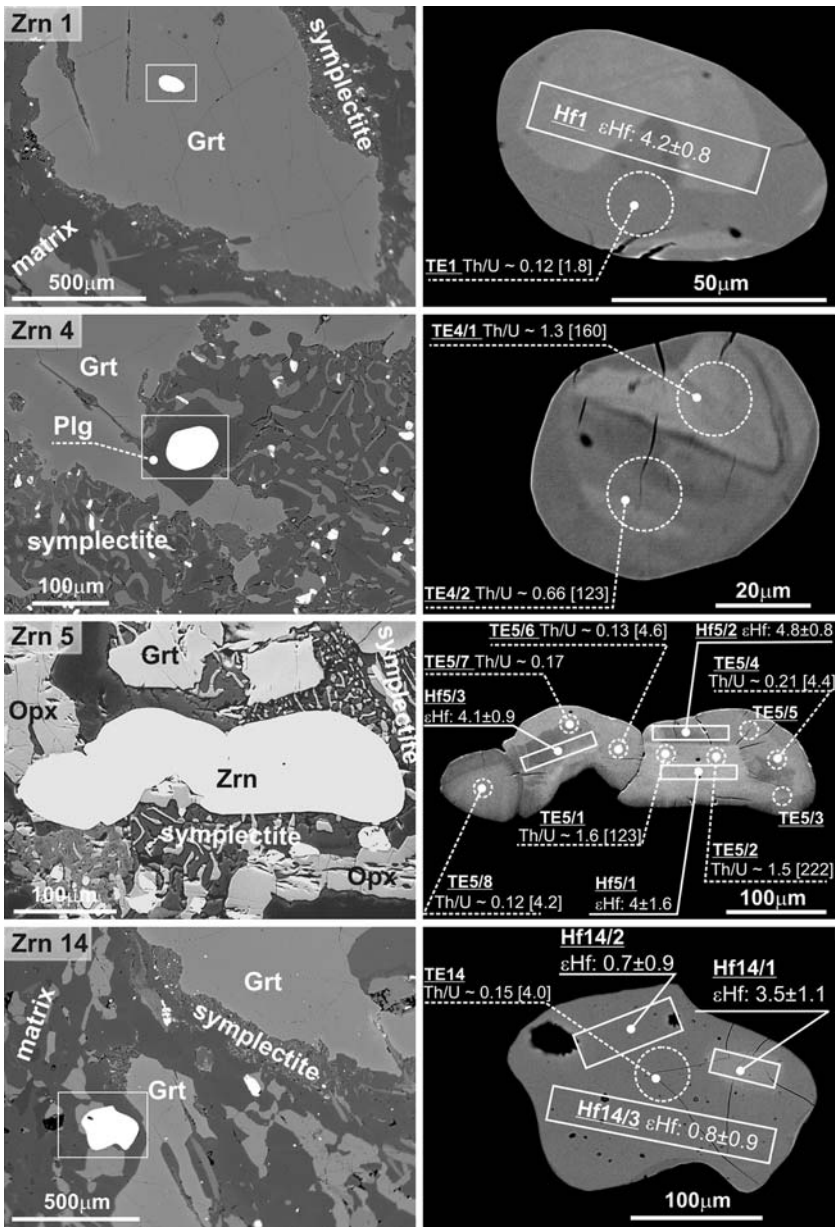

Fig. 6 Textural relationships and BSE images of representative zircon grains in the studied mafic granulite. *Dashed circles* trace elements and REE laser ablation ICP–MS analyses (marked TE) with corresponding Th/U values; Lu_N/Sm_N values in square brackets; *rectangles* laser ablation MC ICP–MS Hf isotopic analyses (marked Hf) with shown εHf values; For images of all measured zircons with their trace elements, REE and Hf isotopic data see Plates 1–4 and ESM_Table 9 in the electronic supplementary material

(Figs. 5g, 6) have lower contents of HREE (La_N/Yb_N ~ 0.01; Lu_N/Sm_N ~ 5.3; Table 2), lower negative Eu anomaly (Eu/Eu* ~ 0.97; Table 2) and lower positive Ce anomaly (Ce/Ce* ~ 7.7; Table 2). The transitional trace element and REE composition of some of the dark-BSE zircon areas (Fig. 5g; zircon 4 in Fig. 6; Table 2) may be indicative of their formation by alteration of the bright-BSE zircon domains. There is no obvious correlation between spatial (textural) position of zircon grains in the studied mafic granulite and their trace element compositions—zircons with high, transitional as well as low REE and trace element contents are located as inclusions in plagioclase, enclosed in garnet, within the reaction products of garnet decay and also in the matrix assemblage (Fig. 6).

Isotopic composition of Hf in minerals

The $^{176}Hf/^{177}Hf$ (εHf) values are reported in Tables 4 and 5. They were all age-corrected using the U–Pb concordia age of 343 ± 2 Ma (2σ, total of 15 laser ablation ICP-MS analyses; Table 3 and Fig. 7). Given the low Lu/Hf ratio in the zircons, the age correction did not have a significant effect on the resulting Hf isotopic composition. The results of in-situ measurements of Hf isotopic composition of zircons by laser ablation MC ICP-MS are plotted in Figs. 6 and 8 combined with the textural relationship of measured zircon in mafic granulite and with trace element and REE characteristics (see also the Plates 1–4 and ESM_Table 9 in the electronic supplementary material). Most of the

Table 3 Laser ablation ICP–MS U–Pb and Pb–Pb data for zircons from the mafic granulite

Analysis	Isotopic ratio						Age (Ma)			
	$^{207}Pb/^{235}U$	1σ	$^{206}Pb/^{238}U$	1σ	$^{207}Pb/^{206}Pb$	1σ	$^{207}Pb/^{235}U$	$\pm1\sigma$	$^{206}Pb/^{238}U$	$\pm1\sigma$
U–Pb 1	0.4126	0.0143	0.0551	0.0006	0.0542	0.0018	351	10	346	4
U–Pb 2	0.4147	0.0115	0.0548	0.0005	0.0546	0.0014	352	8	344	3
U–Pb 3	0.4187	0.0101	0.0543	0.0005	0.0561	0.0014	355	7	341	3
U–Pb 4	0.3768	0.0102	0.0548	0.0007	0.0503	0.0011	325	8	344	4
U–Pb 5	0.4139	0.0097	0.0537	0.0007	0.0561	0.0013	352	7	337	4
U–Pb 6	0.4111	0.0162	0.0539	0.0006	0.0556	0.0019	350	12	339	4
U–Pb 7	0.3874	0.0144	0.0550	0.0008	0.0516	0.0019	332	11	345	5
U–Pb 8	0.4097	0.0110	0.0556	0.0007	0.0526	0.0015	349	8	349	5
U–Pb 9	0.4067	0.0097	0.0551	0.0005	0.0530	0.0013	346	7	346	3
U–Pb 10	0.3982	0.0112	0.0533	0.0006	0.0548	0.0015	340	8	335	3
U–Pb 11	0.4145	0.0096	0.0557	0.0005	0.0536	0.0012	352	7	350	3
U–Pb 12	0.4068	0.0089	0.0551	0.0006	0.0547	0.0011	347	6	346	4
U–Pb 13	0.3886	0.0114	0.0543	0.0007	0.0518	0.0014	333	8	341	4
U–Pb 14	0.4033	0.0204	0.0538	0.0006	0.0548	0.0024	344	15	338	4
U–Pb 15	0.4064	0.0235	0.0549	0.0015	0.0527	0.0030	346	17	345	9

Uncertainties on ages are shown as 1σ in Ma

Table 4 Hf composition of major metamorphic minerals from mafic granulite from Blanský les massif

Mineral	$^{176}Lu/^{177}Hf$	$^{176}Hf/^{177}Hf$	2σ	$^{178}Hf/^{177}Hf$	2σ	$^{180}Hf/^{177}Hf$	2σ	$^{176}Hf/^{177}Hf_{343}$	$\varepsilon\ Hf_{343}$	2σ
Clinopyroxene	0.0136	0.282675	0.000003	1.467183	0.000011	1.886651	0.000021	0.282588	1.02	0.1
Garnet	0.7177	0.287263	0.000004	1.467205	0.000015	1.886675	0.000037	0.282586	0.96	0.1
Rutile in matrix	0.0000	0.282598	0.000007	1.467191	0.000016	1.886619	0.000040	0.282598	1.37	0.2
Biotite	0.0258	0.282760	0.000004	1.467192	0.000017	1.886765	0.000036	0.282595	1.27	0.1
Ilmenite	0.0026	0.282628	0.000007	1.467203	0.000016	1.887076	0.000036	0.282612	1.86	0.3
Rutile in garnet	0.0004	0.282640	0.000010	1.467188	0.000026	1.886510	0.000057	0.282638	2.79	0.4
Amphibole	0.0182	0.282775	0.000006	1.467187	0.000022	1.886692	0.000038	0.282659	3.54	0.2
Orthopyroxene	0.0841	0.283257	0.000010	1.467282	0.000175	1.886824	0.000335	0.282717	5.58	0.3

studied zircons have εHf value in the range of 2.6 to 5.0 (Fig. 8) with only scarce measurements with εHf between 0.7 and 1.3 (Fig. 8). The Hf isotopic composition in zircons does not correlate with neither their chemical, nor their textural properties. Zircons with high εHf values (2.6 to 5.0) are represented by both bright-BSE and dark-BSE zircon domains (often present as bright-BSE zircon core and dark-BSE zircon rim) that are located within the matrix, as inclusions in garnet or plagioclase and also within the reaction products of the garnet decay (Fig. 6). Only few zircons with dark-BSE domains and low trace element and REE contents have low εHf values (0.7 to 1.3) and were found in the matrix (zircon 14 in Fig. 6; Plate 4 in the electronic supplementary material). Such low εHf values were not detected in the bright-BSE areas of zircon grains, nor were they found in zircons enclosed in the garnet.

The Hf isotopic compositions of garnet and other minerals present in the matrix correspond to εHf values of ca. 1 (Table 4). Slightly higher εHf values have been measured in rutile enclosed in the garnet (εHf = 2.8), amphibole (εHf = 3.5) and orthopyroxene (εHf = 5.6). The Hf isotopic composition of ilmenite is more radiogenic compared to the Hf isotopic composition of minerals in the matrix, but its εHf value is lower compared to the εHf values of minerals present in the corona (Table 4). Grains of baddeleyite enclosed in ilmenite were too small to be analysed reliably by laser ablation ICP-MS for Hf isotopes.

Discussion

Garnet corona-forming reaction

The observed garnet consuming decompression reaction, which is characterised by formation of coronitic reaction assemblage around garnet, can be written as:

Table 5 Hf composition of zircon grains from the studied mafic granulite

Zircon	Analysis	Lu/Hf	Yb/Hf	$^{176}Hf/^{177}Hf$	2 σ	$^{178}Hf/^{177}Hf$	2 σ	$^{180}Hf/^{177}Hf$	2 σ	ε Hf_{343}	2 σ
Zrn 1	Hf1	0.0018	0.0303	0.282679	0.000024	1.467189	0.000624	1.886802	0.001676	4.2	0.8
Zrn 2	Hf2	0.0002	0.0030	0.282658	0.000022	1.467380	0.000112	1.886654	0.000194	3.5	0.8
Zrn 5	Hf5/1	0.0106	0.1176	0.282681	0.000044	1.467420	0.000213	1.886529	0.000412	4.0	1.6
Zrn 5	Hf5/2	0.0005	0.0059	0.282696	0.000022	1.467275	0.000171	1.886773	0.000190	4.8	0.8
Zrn 5	Hf5/3	0.0003	0.0037	0.282675	0.000025	1.467263	0.000099	1.886713	0.000127	4.1	0.9
Zrn 6	Hf6	0.0001	0.0020	0.282670	0.000026	1.467226	0.000093	1.886657	0.000179	3.9	0.9
Zrn 7	Hf7	0.0098	0.1353	0.282708	0.000035	1.467285	0.000278	1.886633	0.000350	5.0	1.3
Zrn 8	Hf8/2	0.0001	0.0021	0.282633	0.000025	1.467217	0.000143	1.886445	0.000210	2.6	0.9
Zrn 8	Hf8/3	0.0004	0.0053	0.282655	0.000018	1.467241	0.000106	1.886738	0.000170	3.4	0.6
Zrn 8	Hf8/1	0.0056	0.0819	0.282647	0.000027	1.467198	0.000165	1.886663	0.000234	2.9	0.9
Zrn 9	Hf9/2	0.0002	0.0044	0.282672	0.000029	1.467284	0.000078	1.886782	0.000159	4.0	1.0
Zrn 9	Hf9/1	0.0001	0.0021	0.282666	0.000027	1.467301	0.000105	1.886646	0.000170	3.8	0.9
Zrn 10	Hf10	0.0001	0.0024	0.282689	0.000028	1.467289	0.000136	1.886750	0.000235	4.6	1.0
Zrn 11	Hf11	0.0001	0.0024	0.282685	0.000031	1.467326	0.000129	1.886959	0.000235	4.5	1.1
Zrn 12	Hf12	0.0013	0.0189	0.282598	0.000024	1.467237	0.000088	1.886751	0.000167	1.3	0.9
Zrn 13	Hf13	0.0001	0.0019	0.282587	0.000026	1.467206	0.000115	1.886774	0.000196	1.0	0.9
Zrn 14	Hf14/1	0.0001	0.0019	0.282657	0.000032	1.467191	0.000187	1.886772	0.000414	3.5	1.1
Zrn 14	Hf14/3	0.0001	0.0026	0.282583	0.000025	1.467243	0.000073	1.886798	0.000120	0.8	0.9
Zrn 14	Hf14/2	0.0001	0.0027	0.282579	0.000024	1.467162	0.000082	1.886694	0.000134	0.7	0.9

Numbers of the analyses corresponds to Fig. 6 and Plates 1–4 in the electronic supplementary material

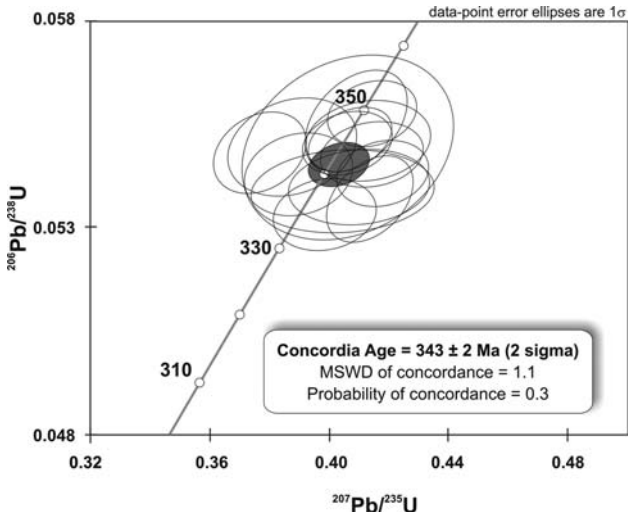

Fig. 7 U–Pb Concordia diagram for zircons from the mafic granulite. Laser ablation ICP–MS data, total of 15 analyses. The concordia age *ellipse* represents 2σ uncertainty, individual analyses are plotted with 1σ uncertainties

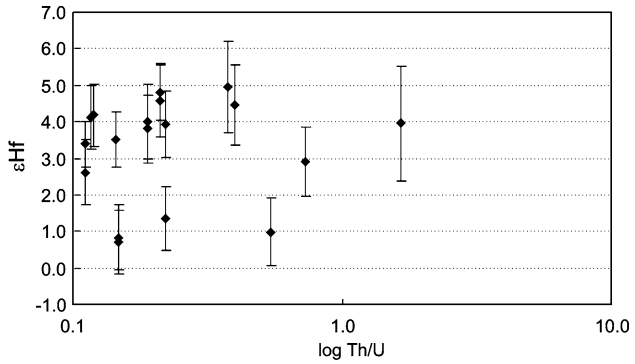

Fig. 8 Hf isotopic composition of zircons from the mafic granulite plotted versus their Th/U values. The corresponding Hf analyses are in Table 5; the uncertainty bars are 2 SE of the Hf isotopic measurements. For a complete set of trace elements, REE and Hf isotopic data of the studied zircons and the textural relationships, see Plates 1–4 and ESM_Table 9 in the journal electronic supplementary material

$$\text{Grt} + \text{Qtz}\ (+\text{Cpx}) = \text{Pl} + \text{Opx} \quad (1)$$

This reaction, previously described from granulites by several authors (e.g. Thost et al. 1991; Owen and Dostal 1996; O'Brien and Rötzler 2003), can be also predicted for the bulk composition of the studied granulite using the pseudosection approach (Fig. 9). The field calculated for the garnet decompression reaction in the P–T space (Fig. 9) is relatively large but using the previously reported P-T-t path for the studied granulites (cf. references in Fig. 9), the P–T conditions of the garnet decompression reaction in the studied mafic granulite can be constrained to approximately 1,000°C and 12–14 kbar.

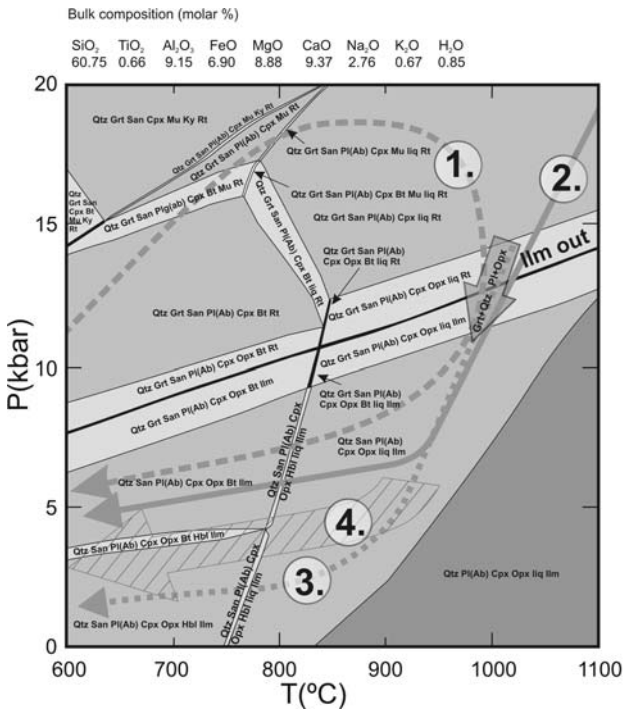

Fig. 9 Calculated P–T pseudosection for the mafic granulite in NCKFMASH–Ti system. P–T paths for the southern Bohemian granulites were adopted from Carswell and O'Brien (1993)—1., Svojtka et al. (2002)—2 and Owen and Dostal (1996)—3. *Line 4* indicates a possible P–T path for the mafic granulite derived from mineral assemblage in the studied sample. Mineral abbreviations are after Kretz (1983)

Using the electron microprobe analyses of reacting phases and minerals produced in the symplectitic part of the reaction corona (zone I; Fig. 2d), the following equation can be written:

$$6\text{Grt} + 3\text{Cpx} = 6\text{An} + 6\text{Opx} + 2\text{Mag} \quad (2)$$

The major element composition of Cpx in the equation is the average composition of Cpx in the matrix; the resulting Opx composition agrees well with the microprobe analyses of Opx grains from the symplectitic rim around the garnet. The major element composition of reacting garnet is difficult to estimate accurately because of strong major element zoning, especially close to the rims and because parts of the rims were consumed during the reaction. The microprobe analysis with the highest Fe and the lowest Ca contents was assumed to be similar to the composition of reacting garnet. The textural observation and compositional study of garnet grains suggest that the major element compositional zoning was not produced as a result of the corona-forming reaction, but rather it represents a pre-corona feature. As a result of the absence of quartz in the reaction (2), magnetite forms on the right side of the equation.

A corresponding equation for the origin of quartz-absent, Pl-Opx (±Hbl)-enriched halo (zone II; Fig. 2d) can be written as:

$$6\text{Grt} + 3\text{Cpx} + 1.44\text{Qtz} = 6\text{An} + 6.72\text{Opx} + 4.56\text{FeO}_{(\text{excess})} \quad (3)$$

Unlike in the reaction (2) where quartz is missing on the left side of the equation, the excess of iron on the right side of the reaction (3) is not compensated for by growth of magnetite and can be assumed to have been accommodated in amphibole. Another receiver of Fe was ilmenite, which formed at the expense of rutile and is represented by infrequent grains occurring in the reaction corona around garnet (Fig. 10b, c). This change was temporally associated with the garnet decay (Fig. 9).

Similar garnet decompression reaction with two contrasting corona assemblages has been previously described from Antarctica by Thost et al. (1991) and interpreted as originating from two stages of metamorphism—the outer corona formed during decompression, the inner corona formed later in response to a minor deformation event. We ascribe the origin of both reaction zones in the studied granulite to only one metamorphic event—the decompression stage of the metamorphic evolution of mafic granulite. We interpret the two contrasting corona assemblages as a result of two different chemical equilibria achieved during the decompression. Firstly, the Pl-Opx (±Hbl) quartz-depleted halo (zone II, Fig. 2) formed by reaction between the garnet rims and the Qtz + Cpx matrix assemblage (Eq. 3). Fluid phase was likely present in the rock during the reaction and buffered the activity of Fe. It probably also activated the reaction because the reaction products are only found outside the garnet grains but never within the garnet, despite the presence of quartz and clinopyroxene inclusions that would be expected to react. Later, the An + Opx + Mag symplectitic assemblage (zone I in Fig. 2d, Eq. 2) formed following the quartz depletion in the matrix assemblage. The formation of magnetite in the rock suggests a low activity of fluids, which could otherwise carry the excess Fe away from the place of reaction. This could have been caused by a shielding effect of zone II of the reaction corona.

Redistribution of Zr and other elements during the reaction

Assuming a closed system for Zr in the studied granulite, a simple mass balance calculation can be used to decipher the Zr behavior and its re-distribution between reactants and products during the metamorphic reactions. Reaction (4) describes only those phases that contain significant amounts of Zr:

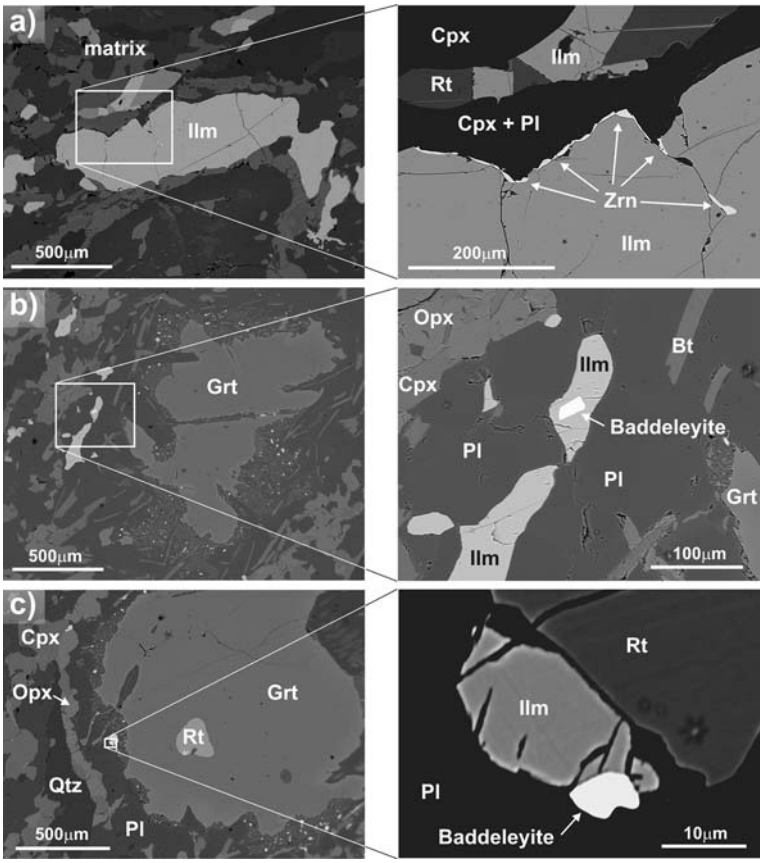

Fig. 10 Distribution of Zr–rich phases in ilmenite. **a** small flat zircons at the rim and in the crack of a large ilmenite grain of the first generation. The ilmenite grain in the upper part of the figure formed from the adjacent rutile; **b** small ilmenite grain with a baddeleyite inclusion near the reaction corona around garnet, the ilmenite formed probably from rutile and represents the second generation of ilmenite in the mafic granulite; **c** rutile grain in the reaction corona around garnet that has been partly transformed to ilmenite and baddeleyite

$$2\text{Grt}\ (Zr_{aver} = 20\ \text{ppm}) + 1\text{Cpx}\ (Zr_{aver} = 109\ \text{ppm}) = 2\text{Opx}\ (Zr_{aver} = 7\ \text{ppm}) \quad (4)$$

The petrographical study of mafic granulite suggests that approximately 50% of the garnet (~10 wt% of the rock) reacted during the decompression reaction. The Eq. (4) is expressed in mole units; it is therefore possible to write another Eq. (5), which shows the reaction with respect to the weight percents of individual Zr-bearing minerals:

$$10\%_{wt}\ \text{Grt}(20\ \text{ppm Zr}) + 2.44\%_{wt}\ \text{Cpx}(109\ \text{ppm Zr}) = 4.86\%_{wt}\ \text{Opx}(7\ \text{ppm Zr})$$
(weight percents refer to the whole rock = 100 % wt) (5)

The calculated mineral proportions agree well with the observed abundance of orthopyroxene in the rock (~5 wt%) and they are consistent with its origin exclusively from the garnet decompression reaction.

Taking the Zr concentration in the whole rock (51 ppm) as 100% of Zr content, the following Zr mass balance can be written for the garnet decompression reaction based on Eq. (5):

$$9.1\%_{\text{whole rock}}\ \text{Zr[left side of reaction (5)]} = 0.7\%_{\text{whole rock}}\ \text{Zr[right side of reaction (5)]} \quad (6)$$

This is a Zr-releasing reaction with excess of 8.4% of the whole rock Zr content on the product side of the equation.

The excess Zr released during this reaction can either be accommodated in other mineral phases as a trace constituent, or it can contribute to the newly formed zircon. In order to assess which of the mechanisms was dominant in the studied mafic granulites, the trace element distribution and textural relationships between Zr-bearing minerals in the reaction products of the garnet decay have been studied.

Because Zr is generally considered to be immobile in most geological environments, it is expected that the newly formed zircons would grow close in space to the Zr-releasing reaction in the rock. This process has been documented by Degeling et al. (2001) from garnetiferous migmatites in SW Norway, where numerous small zircons of up to 20 microns in size grew directly in the cordierite corona that formed as a result of garnet decompression decay. In-situ growth of zircon from garnet and ilmenite was described also by Fraser et al. (1997) and Bingen et al. (2001), respectively. In this study, the in-situ crystallization

of zircon in the reaction corona was not observed in the mafic granulite and even the large zircon crystals present in the products of the garnet decay (zircon 5 in Fig. 6) show effects of deformation and alteration rather than crystallization of new zircon.

It is therefore likely that the other major mineral phases that have participated in the reaction could have accommodated all the released Zr. It can be calculated that amphibole (~3 wt% of the rock, ~210 ppm Zr) has a potential to accommodate the whole amount of Zr released during the garnet decay reaction (see also Fraser et al. 1997). The higher Zr content in amphiboles that are spatially associated with the reaction corona in the studied granulite, compared to the amphibole grains in the matrix clearly shows an increased Zr activity in the vicinity of garnet during the decompression reaction and a buffering activity of the fluid phase (now represented by amphibole) for the excess Zr in the system.

Another Zr-bearing phase that participated in the decompression reaction is rutile, which was partially transformed to ilmenite. This reaction is related to the Fe release during the decompression reaction [Fe excess on the right side of the Eq. (3)] The presence of ovoid shape ilmenite (typical shape of rutile enclosed in garnet) in the proximity of garnet reaction rim indicates that this reaction was simultaneous with the garnet decay. The incomplete transformation of rutile to ilmenite is common (Fig. 10a, c) and its progress probably depends on the Fe influx from the garnet decay reaction. Because rutile is a Zr-rich phase (up to ~6,600 ppm Zr; Table 2) and because it was transformed to ilmenite with significantly lower content of Zr (~55–150 ppm Zr; Table 2), small euhedral baddeleyite grains are now present in some ilmenite grains (Fig. 10b, c). This is indicative of a limited ability of ilmenite to accommodate Zr in its crystal lattice during retrograde stage of metamorphism, a feature that has been described from magmatic ilmenites from Greenland as a consequence of subsolidus magma cooling (Naslund 1987).

Typical of the studied granulite is the presence of small elongated or flat zircon grains that make a discontinuous rim around some larger ilmenite grains (Fig. 10a). A similar zircon occurrence was described by Bingen et al. (2001) from granulites and eclogites. They explained the zircon presence by its formation from baddeleyite, which originated from exsolution of a magmatic ilmenite. During the granulite facies conditions, this baddeleyite was transformed to zircon by an increased activity of SiO_2 in the system. However, in the studied granulite there seem to be neither spatial, nor temporal association of zircon with baddeleyite and ilmenite. Should the observed baddeleyites in small ilmenite grains be precursors of the coronitic zircons around the larger ilmenite grains, at least some relics of baddeleyite from an incomplete transformation to zircon would be present in the rock. In addition, the influx of Si due to the increased activity of SiO_2 would not affect the baddeleyite enclosed in ilmenite, but it would rather transform the baddeleyite that is present outside the ilmenite grains. Since the studied granulite contains baddeleyite with no indication of its transformation to zircon, two populations of ilmenite that formed by different processes and that have a different effect on the Zr budget can be distinguished:

1. Larger ilmenite grains in the matrix with originally high content of Zr that was released during the granulite facies metamorphism and accommodated by coronitic zircon (Fig. 10a; cf. Bingen et al. 2001).
2. Smaller ilmenite grains in the matrix (Fig. 10b) as well as in the reaction coronas around garnet (Fig. 10c) which can contain relics of rutile, and some of the ilmenites have shapes suggesting their rutile precursors. The excess of Fe formed as a result of garnet consumption during the decompression was probably accommodated by transformation of rutile into ilmenite. The occurrence of baddeleyite in this ilmenite can be caused by a reduced capacity of ilmenite to bind Zr (cf. the larger, Zr-rich ilmenite grains that changed to Zr-poor ilmenite rimmed by zircon). An example is shown in Fig. 10c where rutile in the reaction zone of the garnet corona is partially changed to ilmenite with a small newly formed grain of baddeleyite. The major and trace element compositions of two ilmenite populations are very similar and accordingly, only the type of inclusions and the size and morphology can be used to tell the two different ilmenite generations apart.

Collectively, the Zr balance for the garnet-consuming and Zr-releasing reaction observed in the studied mafic granulite is difficult to decipher fully as it might have been affected by multiple processes with several potential Zr donors and receivers. There is no indication of newly grown zircon spatially associated with the corona reaction around the garnet, although the reaction results in release of a significant amount of Zr. It is more likely that the Zr was stored in the fluid phase (amphibole), which played an important role in the reaction and could also have transported some elements, such as Fe, and enable the transformation of rutile to ilmenite. The contribution of Zr (and Hf) from rutile to the fluid phase during the transformation to ilmenite is unlikely since the Zr content in the amphibole reflects the amount of Zr-released exclusively from the garnet decayed during the decompression reaction. The Zr-content of rutile was retained by formation of baddeleyite inclusions in the newly formed ilmenite.

Distribution of trace elements and REE between minerals

It has been documented in a number of studies that distribution of trace elements and REE in zircon reflects the metamorphic history of the rocks and that the individual zircon growth stages can be associated with specific metamorphic conditions (e.g. Schaltegger et al. 1999; Rubatto 2002; Möller et al. 2002; Hermann and Rubatto 2003; Whitehouse and Platt 2003; Hokada and Harley 2004; Kelly and Harley 2005). In general, high contents of trace elements and REE (especially HREE) in zircon are believed to reflect its magmatic origin (Williams et al. 1996; Schaltegger et al. 1999; Hoskin and Black 2000; Rubatto 2002; Hermann and Rubatto 2003). Low trace element and REE contents have been described from metamorphic zircons (e.g. Williams et al. 1996; Schaltegger et al. 1999; Hermann and Rubatto 2003; Rubatto 2002; Whitehouse and Platt 2003; Kelly and Harley 2005) but the recent studies revealed (Hoskin and Schaltegger 2003; Hoskin 2005; Geisler et al. 2007) that trace element and REE composition of zircon strongly depends on the composition of the coexisting fluid phase (or melt), commonly present in the crust during HP-HT metamorphism. Number of geochemical parameters has been suggested for discriminating between diverse zircon populations growing under different chemical and P–T conditions, in particular the Th/U ratio and the partition coefficients between coexisting zircon and garnet ($^{REE}D_{Zrn/Grt}$).

Two types of zircon can be distinguished in the studied mafic granulite, based on the results of BSE imaging. The bright-BSE zircon domains are characterized by high content of trace elements, especially Y, Th, U and Th/U value of ~1.2 (Table 2 and Fig. 6; see also Plates 1–4 and ESM_Table 9 in the electronic supplementary material). The calculated $^{Gd}D_{Zrn/Grt}$ ~ 2.1 to $^{Lu}D_{Zrn/Grt}$ ~ 99 (Fig. 11) have values higher than those reported for metamorphic zircon growing in equilibrium with garnet (Rubatto 2002; Whitehouse and Platt 2003; Kelly and Harley 2005). It is therefore likely that the bright-BSE zircon zones did not form in equilibrium with the garnet and probably represent zircon of magmatic origin.

The dark-BSE zircon domains have usually low contents of trace elements with Th/U ratios in the range of 0.1–0.5 (Table 2 and Fig. 6; Plates 1–4 and ESM_Table 9 in the electronic supplementary material). The calculated partition coefficients for HREE (Fig. 11) show a typical pattern for zircon growing in the presence of garnet (Rubatto 2002; Whitehouse and Platt 2003; Hokada and Harley 2004; Kelly and Harley 2005), which sequester HREE from the system causing HREE depletion in concurrently growing zircon. When compared to the values of partition coefficients published previously for LREE in zircon growing in equilibrium with garnet (Rubatto 2002; Hokada and Harley 2004), our data show systematically lower values of calculated $D_{Zrn/Grt}$ for La, Ce Pr and Nd (Fig. 11). This apparent discrepancy may be due to differences in bulk composition and presence or lack of other REE-rich phases in rocks studied here (mafic granulites) and in the previous studies (felsic granulites). More experimental data are needed to assess the effects of composition and presence of concomitant mineral phases on the values of $^{REE}D_{Zrn/Grt}$.

The presence of zircons with low trace element and REE content enclosed in the garnet suggests that this zircon had to form before the growth of garnet. The presence of zircons with bright-BSE (high trace element and REE contents) patches and dark-BSE (low trace element and REE contents) zones with ghost zoning suggest that transformation of older, bright-BSE zircon, rather than growth of zircon in equilibrium with garnet, resulted in the formation of dark-BSE zircon domains. This type of zircon has been found both in the matrix assemblage and enclosed in the fresh garnet (Fig. 6; Plates 1-4 in the electronic supplementary material).

Similarly, the Th/U ratio, which decreases from the bright-BSE zircons (Th/U ~ 1.2) to the dark-BSE zircons (Th/U ~ 0.2) with transitional values (Th/U ~ 0.5, Table 2) in zircon domains with ghost zoning has been shown to form during alteration of magmatic zircon (Vavra et al. 1999; Hoskin and Black 2000; Möller et al. 2002). However, using the Th/U value in zircon to define its magmatic or metamorphic origin has been recently disputed (Hermann 2002; Möller et al. 2002; Bingen et al. 2004; Kelly and Harley 2005).

The dark-BSE zircon domains reveal ghost or fading zoning indicating recrystallization of older, trace element rich zircon (Hoskin and Black 2000). Although the study of Hoskin and Black (2000) showed significant decrease of LREE in the recrystallized domains, the opposite trend, decrease in HREE, which is consistent with our observations (Fig. 5g), was described by Kelly and Harley (2005) from recrystallized magmatic zircons from Zircon Point paragneisses in the Napier Complex (Antarctica). The composition of fluid, which usually triggers the zircon alteration, strongly influences the trace element and REE composition of altered zircon (Hoskin and Black 2000; Hoskin and Schaltegger 2003; Hoskin 2005; Pettke et al. 2005; Geisler et al. 2007).

Trace element concentrations in other studied minerals depend primarily on their spatial relations and distance from the garnet corona that acted as a source of trace elements and REE during decompression. In the amphibole it is not only Zr, but also Y, Th, Hf, U and HREE that have higher concentrations in the grains within the garnet reaction zone II compared to the amphibole grains in the matrix, away from the reaction corona (Table 1). It suggests a

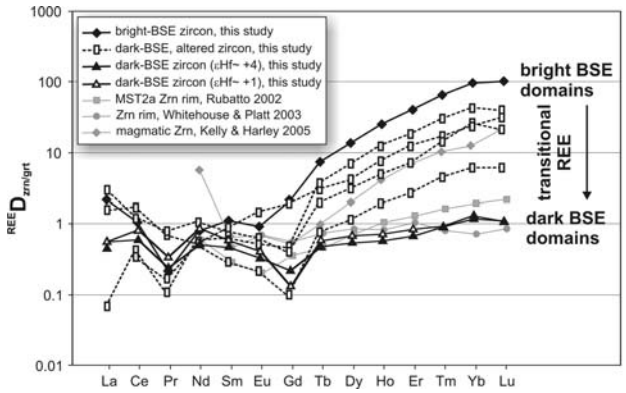

Fig. 11 Calculated REE partition coefficients for zircon–garnet pairs in the mafic granulite. $^{REE}D_{Zrn/Grt}$ = REEzircon/REEgarnet, using REE concentrations measured by laser ablation ICP–MS. Except for the dark–BSE altered zircon that represent individual analyses, partition coefficients of other studied zircon types were calculated using their average REE concentrations (Table 2; for a complete set of REE data in zircon, see ESM_Table 9 in the journal electronic supplementary material). Partition coefficient data of coexisting metamorphic zircon and garnet from other authors are plotted for comparison; $^{REE}D_{Zrn/Grt}$ data of Kelly and Harley (2005) are for magmatic zircon

contribution of these elements from the decaying garnet to the coexisting fluid phase and later to the newly formed amphibole.

Garnet is characterized by zoning of the Zr content, which increases from the core to the rim and by zoning of some of the REE that follow an opposite trend and their contents decrease towards the rim (Fig. 3). This is consistent with the observed major element zoning and it is indicative of a prograde garnet growth. Some garnet grains have a thin retrograde almandine-rich rim, which was too small to be analyzed for a possible trace element zoning because of the limited spatial resolution of the LA ICP-MS measurements. The positive Ce anomaly in the studied garnet (Fig. 5a) suggests that the system was enriched in Ce during the garnet growth and that there was no other concomitant phase (e.g. zircon), which would preferentially bind Ce. The elevated Ce content is consistent with disequilibrium between garnet and zircon during the garnet growth.

Variations in the trace element contents in rutile are potentially important because of the high content of Zr in rutile. Zack et al. (2004) found that rutile grains in the matrix of UHT (>700°C) rocks have a significantly lower Zr content compared to rutiles enclosed in the garnet and suggested their growth or reequilibration along a retrograde P–T path. In contrast, the anhedral rutile grains in the matrix of the studied mafic granulite have higher Zr contents compared to the rutile enclosed in the garnet. This apparent discrepancy between our observation and the rutile composition described in Zack et al. (2004) may have resulted from the rutile crystallization in equilibrium with a melt phase that was rich in trace elements and the presence of which is considered to be common in the granulite facies rocks (Roberts and Finger 1997; Finger and Cooke 2004; Tropper et al. 2005). As the melt evolution progresses along a retrograde P–T path, the melt becomes trace element-supersaturated and starts to crystallize accessory minerals (Roberts and Finger 1997; Finger and Cooke 2004; Tropper et al. 2005). Tropper et al. (2005) suggested this mechanism for the formation of anhedral rutiles that are common in the matrix of many Moldanubian granulites. The textural relations in the studied granulite suggest that the growth of anhedral rutile had to take place before or simultaneously with the transformation of rutile to ilmenite during the decompression of the granulites. Calculated temperature using the Zr-in-rutile thermometer (Watson et al. 2006) yielded temperature of 993°C for the rutile grain with the highest Zr content in the matrix. This value agrees well with the peak temperatures proposed for the Moldanubian granulites by Carswell and O'Brien (1993) and Owen and Dostal (1996). A similar calculation using the calibration of Zack et al. (2004) yielded a higher temperature of ca. 1,100°C. The observed difference between our two temperature estimates can be explained by calibration of Zack's thermometer using rutile grains enclosed in garnet that could have possibly been affected by diffusive isolation from zircon (Watson et al. 2006).

Biotite has a very low concentration of trace elements, including the REE. It is assumed that it formed during the granulite retrogression and a later influx of fluids, and that the formation of biotite is not related to the garnet decompression reaction (cf. Fig. 9). The localized variations in trace element and REE concentrations in the biotite may have been caused by fluid leaching of trace elements from the coexisting trace element- and REE-rich phases. This is consistent with increased concentrations of a number of trace elements and REE in the biotite grains that are immediately adjacent to the ilmenite (cf. Table 1).

Evolution of Hf isotopes and zircon behaviour during metamorphism

The Hf isotopic evolution of individual phases in the rock can be used to trace back the potential metamorphic reactions and their timing as shown in Fig. 12, where the Hf evolution trends of major minerals are plotted as εHf values against the time. The Hf isotopic compositions for garnet, clinopyroxene, biotite and rutile from the matrix intersect at ca. 343 Ma (i.e. U–Pb age of zircons), corresponding to the εHf value of ca. 1. From these minerals, only garnet has a sufficiently high Lu/Hf ratio that can result in a significant change of εHf over time. As a result, Hf released during the garnet dissolution can have a sig-

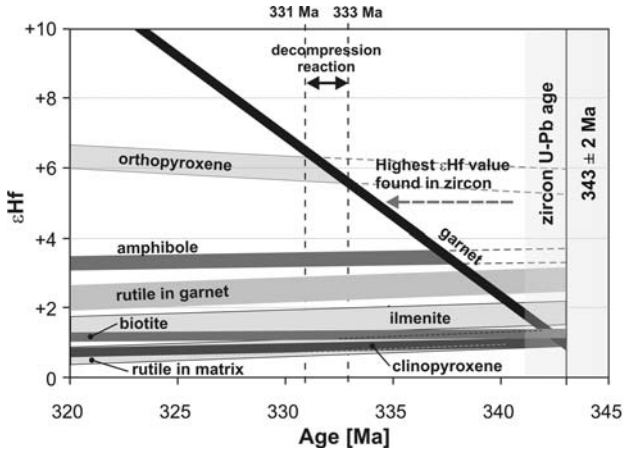

Fig. 12 Time evolution of Hf isotopes for individual minerals in the studied mafic granulite. The bands represent Hf evolution trends in minerals calculated using the values from Table 4; widths of the bands are 2σ of the εHf values

nificant effect on the Hf isotopic composition of the newly formed minerals. This can be seen in Fig. 12 where amphibole and orthopyroxene have higher calculated εHf_{343} values compared to other minerals, suggesting their different crystallization age and/or source of Hf. Compared to their host, the rutile inclusions in garnet have a higher εHf_{343} value (ca. 2.8). When garnet dissolves and rutile is involved in the reaction, its Hf isotopic composition, together with the Hf released from the garnet, can affect the Hf isotopic composition of the newly-formed amphibole, orthopyroxene and zircon. The presence of two isotopically different sources of Hf within the garnet makes it difficult to estimate the isotopic composition of Hf released during the decompression reaction. It can be assumed that some of Hf released from rutile was retained in baddeleyite that now forms small inclusions in ilmenite. Differences in the εHf values calculated for orthopyroxene and amphibole (ca. 5.6 and 3.5, respectively, Fig. 12) can be explained by different contributions from garnet and rutile to the Hf contained in these two minerals that formed during the garnet decay as a result of decompression. The Hf isotopic evolution of orthopyroxene also constrains the maximum age of garnet breakdown during the decompression to ca. 333–331 Ma (2σ interval in Fig. 12) for which P (12–14 kbar) and T (~1,000°C) were estimated from the pseudosection (Fig. 9). The estimated age for the decompression based on the evolution of Hf isotopes is significantly younger than the LA ICP-MS U–Pb zircon age of 343 ± 2 Ma (Fig. 7) and than most of the U–Pb ages of zircons reported in the literature for granulite facies metamorphism in the southern Bohemian Massif.

Variations in the Hf isotopic composition of zircons does not correlate with the variations in their trace element contents and it cannot be used to distinguish between the bright-BSE trace element rich and the dark-BSE trace element poor domains in the zircon grains. The εHf values for the bright-BSE parts of zircons present in the matrix and as inclusions in the garnet (e.g. zircon 5 in Fig. 6; Plates 2–4 in the electronic supplementary material) vary between 2.6 and 5.0. The dark-BSE and trace element poor zircon domains in these zircons that have most likely formed by zircon recrystallization (e.g. zircon 5 in Fig. 6; Plates 1–3 in the electronic supplementary material) have Hf isotopic composition identical with the bright-BSE parts of zircons. The most likely explanation for this similarity between the otherwise compositionally different zircon domains is the Hf immobility during zircon recrystallization (Kinny and Maas 2003). Zircons that are dominantly dark-BSE and occur in the matrix have contrasting εHf values of 0.7 to 1.3 (e.g. zircon 14 in Fig. 6; Plate 4 in the electronic supplementary material). Differences in the Hf isotopic composition between these two groups of zircons cannot be easily explained on the basis of the first group forming as a result of garnet decompression and the second group representing the pre-decompression mineral assemblage in the mafic granulite namely because some of the first group zircons are enclosed in the garnet.

Collectively, the Hf isotopic composition of zircons in the studied mafic granulite is difficult to interpret in the context of the metamorphic crystallization of other mineral phases in this rock but rather it reflects its pre-decompression chemical and phase composition.

Conclusions

The study of Hf isotopes in metamorphic rocks and minerals has a strong potential for deciphering the metamorphic evolution and it complements other techniques of metamorphic petrology. It can be demonstrated that conventional approach using chemical analyses and compositional imaging, such as backscattered electrons or cathodoluminiscence, to interpret zircon U–Pb age data is limited in that it does not provide sufficient information on the potential sources of Zr for the newly grown zircons. Variation in the Hf isotopic composition of zircons and its comparison to the evolution of Hf in other phases in the can be potentially used to link the growth of zircon to specific metamorphic reactions but in the present study, the formation of zircons could not be related to the latest (decompression) phase of the metamorphic evolution of the mafic granulite.

The presence of amphibole with high content of Zr suggests that some of Zr released during the decomposition of garnet has been sequestered in the fluid phase. The excess of Zr from rutile to ilmenite reaction was accommodated by formation of baddeleyite inclusions in ilmenite.

The study of Hf isotopic evolution of minerals in the mafic granulites provided a time estimate for the garnet decompression reaction for which the P–T conditions were calculated using the pseudosection method at $P = 12$–14 kbar and $T = 1{,}000$°C. The age for the granulite decompression was calculated between 333 and 331 Ma, i.e. ca. 7 Ma younger than the available U–Pb zircon ages from the Moldanubian granulites.

Collectively, the combination of Hf isotopic, trace element and petrological study of minerals provides us with an excellent tool to decipher the metamorphic crystallization and reaction histories of highly metamorphosed rocks. It allows assessing the redistribution of elements during metamorphic processes and relation of the reactions to the crystallization of geochronologically important accessory phases, such as is the zircon.

Acknowledgments This project has been financially supported by the Czech Science Foundation—grant 205/05/0381 and Grant Agency of the Charles University—grant 264/2005/B-GEO. J. Franěk is thanked for providing granulite samples necessary for the study and L. Tajčmanová for help with pseudosection calculation. Ole Tumyr, Hildegunn Almelid and Yuval Ronen provided laboratory assistance in Bergen. The ICP-MS facility at Bergen University is supported by Research Council of Norway. The authors would like to thank S. Harley and U. Schaltegger for careful and constructive reviews of this manuscript.

References

Aftalion M, Bowes DR, Vrána S (1989) Early Carboniferous U–Pb zircon age of garnetiferous, perpotassic granulites, Blanský les massif, Czechoslovakia. Neues Jahrbuch für Mineralogie, Monatshefte 4:145–152

Andersen CA, Hinthorne JR (1972) U, Th, Pb and REE abundances and 207Pb/206Pb ages of individual minerals in returned lunar material by ion microprobe mass analysis. Earth Planet Sci Lett 14:195–200

Andersen T, Griffin WL (2004) Lu-Hf and U-Pb isotope systematics of zircon from the Storgangen Intrusive Complex, SW Norway; implications for the composition and evolution of Precambrian lower crust in the Baltic Shield. Lithos 73:271–288

Bingen B, Austrheim H, Whitehouse M (2001) Ilmenite as a source for zirconium during high-grade metamorphism? Textural evidence from the Caledonides of W. Norway and implications for zircon geochronology. J Petrol 42:355–375

Bingen B, Austrheim H, Whitehouse MJ, Davis WJ (2004) Trace element signature and U–Pb geochronology of eclogite-facies zircon, Bergen Arcs, Caledonides of W Norway. Contrib Mineral Petrol 147: 671–683

Blichert-Toft J, Albarède F (1997) The Lu–Hf isotope geochemistry of chondrites and the evolution of the mantle-crust system. Earth Planet Sci Lett 148:243–258

Carswell DA, O'Brien PJ (1993) Thermobarometry and geotectonic significance of high-pressure granulites: examples from the Moldanubian zone of the Bohemian Massif in Lower Austria. J Petrol 34:427–459

Cherniak DJ, Hanchar JM, Watson EB (1997) Diffusion of tetravalent cations in zircon. Contrib Mineral Petrol 127:383–390

Compston W (1996) SHRIMP: origins, impact and continuing evolution. J R Soc West Austr 79:109–117

Compston W, Williams IS, Meyer C (1984) U–Pb geochronology of zircons from Lunar breccia 73217 using a sensitive high mass-resolution ion microprobe. J Geophys Res 89B:525–534

Cooke RA (2000) High-pressure/temperature metamorphism in the St. Leonhard Granulite Massif, Austria: evidence from intermediate pyroxene-bearing granulites Int J Earth Sci 89:631–651

Dallmeyer RD, Franke W, Weber K (eds) (1995) Pre-permian geology of Central and Eastern Europe. Springer, Berlin

DeBièvre P, Taylor PDP (1993) Table of the isotopic composition of the elements. Int J Mass Spectrom Ion Process 123:149–166

Degeling H, Eggins S, Ellis DJ (2001) Zr budgets for metamorphic reactions, and the formation of zircon from garnet breakdown. Mineral Mag 65:749–758

Fiala J, Fuchs G, Wendt JI (1995) Moldanubian zone—stratigraphy. In: Dallmeyer RD, Franke W, Weber K (eds) Pre-permian geology of Central and Eastern Europe. Springer, Berlin, pp 417–428

Fiala J, Matějovská O, Vaňková V (1987) Moldanubian granulites and related rocks: petrology, geochemistry, and radioactivity. Rozpravy Ceskoslovenske akademie ved, rada matematickych a prırodnıch ved 97:1–102

Finger F, Cooke RA (2004) Evidence for the presence of a trace-element-loaded interstitial partial melt in a moldanubian leucocratic granulite derived from LA-ICP-MS analyses of zircons and rutiles. International workshop on petrogenesis of granulites and related rocks, Náměšť nad Oslavou, 1–3 October 2004, special publication of the Moravian Museum in Brno, pp 35–36

Franke W (1989) Tectonostratigraphic units in the Variscan Belt of Central Europe. Geol Soc Am Spec Pap 230:67–90

Franke W (2000) The mid-European segment of the Variscides: tectonostratigraphic units, terrane boundaries and plate tectonic evolution. In: Franke W, Haak V, Oncken O, Tanner D (eds) Orogenic processes: quantification and modelling in the Variscan Belt. Geological Society, London, Special Publication 179. Geological Society, London, pp 35–61

Fraser G, Ellis D, Eggins S (1997) Zirconium abundance in granulite-facies minerals, with implications for zircon geochronology in high-grade rocks. Geology 25:607–610

Friedl G, Cooke R, Finger F, McNaughton NJ, Fletcher A (2003) U–Pb SHRIMP dating and trace element investigations on multiple zoned zircons from a South-Bohemian granulite. J Czech Geol Soc 48:51–52

Fuchs G, Matura M (1976) Zur Geologie des Kristallins der süddlichen Böhmishe Masse. Jahr Geol Bund 119:1–43

Geisler T, Schaltegger U, Tomaschek F (2007) Re-equilibration of zircon in aqueous fluids and melts. Elements 3:43–50

Griffin WL, Pearson NJ, Belousova E, Jackson SE, van Achterbergh E, O'Reilly SY, Shee SR (2000) The Hf isotope composition of cratonic mantle: LAM-MC-ICPMS analysis of zircon megacrysts in kimberlites. Geochim Cosmochim Acta 64:133–147

Hermann J (2002) Allanite: thorium and light rare earth element carrier in subducted crust. Chem Geol 192:289–306

Hermann J, Rubatto D (2003) Relating zircon and monazite domains to garnet growth zones: age and duration of granulite facies metamorphism in the Val Malenco lower crust. J Met Geol 21:833–852

Hirata T, Nesbitt RW (1995) U–Pb isotope geochronology of zircon: evaluation of the laser probe-inductively coupled plasma mass spectrometry technique. Geochim Cosmochim Acta 59:2491–2500

Hokada T, Harley SL (2004) Zircon growth in UHT leucosome: constraints from zircon-garnet rare earth elements (REE) relations in Napier Complex, East Antarctica. J Mineral Petrol Sci 99:180–190

Hoskin PWO (2005) Trace-element composition of hydrothermal zircon and the alteration of Hadean zircon from the Jack Hills, Australia. Geochim Cosmochim Acta 69(3):637–648

Hoskin PWO, Black LP (2000) Metamorphic zircon formation by solid-state recrystallization of protolith igneous zircon. J Met Geol 18:423–439

Hoskin PWO, Schaltegger U (2003) The composition of zircon and igneous and metamorphic petrogenesis. Rev Mineral Geochem 53:27–62

Jackson SE, Longerich HP, Dunning R, Fryer BJ (1992) The application of laser-ablation microprobe-inductively coupled plasma mass spectrometry LAM-ICP-MS to in situ trace element determinations in minerals. Can Mineral 30:1049–1064

Jackson SE, Longerich HP, Horn I, Dunning R (1996) The application of laser ablation microprobe (LAM)-ICP-MS to in situ U–Pb zircon geochronology. J Conf Abstr 1:283

Janoušek V, Finger F, Roberts M, Frýda J, Pin Ch, Dolejš D (2004) Deciphering the petrogenesis of deeply buried granites: whole-rock geochemical constraints on the origin of largely undepleted felsic granulites from the Moldanubian Zone of the Bohemian Massif. Trans R Soc Edinb Earth Sci 95:141–159

Kelly NM, Harley SL (2005) An integrated microtextural and chemical approach to zircon geochronology: refining the Archaean history of the Napier Complex, east Antarctica. Contrib Mineral Petrol 149(1):57–84

Kinny PD, Maas R (2003) Lu–Hf and Sm–Nd isotope systems in zircon. Rev Mineral Petrol 53:327–341

Koepke J, Behrens H (2001) Trace element diffusion in andesitic melts: an application of synchrotron X-ray fluorescence analysis. Geochim Cosmochim Acta 65(9):1481–1498

Košler J, Fonneland H, Sylvester P, Tubrett M, Pedersen RB (2002) U–Pb dating of detrital zircons for sediment provenance studies—a comparison of laser ablation ICPMS and SIMS techniques. Chem Geol 182:605–618

Košler J, Sylvester PJ (2003) Present trends and the future of zircon in geochronology: laser ablation ICP-MS. Rev Mineral Geochem 53:243-275

Kotková J, Gerdes A, Parrish RR, Novák M (2003) Pressure–temperature–time evolution of granulite clasts from Lower Carboniferous conglomerates—evidence for rapid exhumation at the eastern margin of the Variscan Bohemian Massif. Geophys Res Abstr 5:434

Kotková J, Harley SL (1997) Mineral controls on the trace element and REE geochemistry of high-pressure leucogranulites from the Bohemian Massif. J Czech Geol Soc 42:40

Kretz R (1983) Symbols for rock forming minerals. Am Mineral 68:277–279

Kröner A, O'Brien PJ, Nemchin AA, Pidgeon RT (2000) Zircon ages for high pressure granulites from South Bohemia, Czech Republic, and their connection to Carboniferous high temperature processes. Contrib Mineral Petrol 138:127–142

Kröner A, Wendt I, Liew TC, Compston W, Todt W, Fiala J, Vaňková V, Vaněk J (1988) U–Pb zircon and Sm–Nd model ages of high-grade Moldanubian metasediments, Bohemian Massif, Czechoslovakia. Contrib Mineral Petrol 99:257–266

Lapen TJ, Mahlen NJ, Johnson CM, Beard BL (2004) High precision Lu and Hf isotope analyses of both spiked and unspiked samples: a new approach. Geochem Geophys Geosyst 5. doi:10.1029/2003GC000582

Ludwig KR (2003) User's manual for Isoplot v. 3.00, a geochronological toolkit for Microsoft Excel, Berkeley Geochronological Center, Special Publication no. 4

Matte P, Maluski H, Rajlich P, Franke W (1990) Terrane boundaries in the Bohemian Massif: result of large-scale Variscan shearing. Tectonophysics 177:151–170

Mezger K, Krogstad EJ (1997) Interpretation of discordant U–Pb zircon ages: an evaluation. J Met Geol 15:127–140

Möller A, O'Brien PJ, Kennedy A, Kröner A (2002) Polyphase zircon in ultrahigh-temperature granulites (Rogaland, SW Norway) constraints for Pb diffusion in zircon. J Met Geol 20:727–740

Munker C, Weyer S, Scherer E, Mezger K (2001) Separation of high field strength elements (Nb, Ta, Zr, Hf) and Lu from rock samples for MC-ICP-MS measurements, Geochem Geophys Geosyst 2 (12). doi:10.1029/2001GC000183

Naslund HR (1987) Lamellae of baddeleyite and Fe-Cr-spinel in ilmenite from the Basistoppen sill, East Greenland. Can Mineral 25:91–96

O'Brien PJ, Rötzler J (2003) High-pressure granulites: formation, recovery of peak conditions and implications for tectonics. J Met Geol 21:3–20

O'Brien PJ, Vrána S (1995) Eclogites with a short-lived granulite facies overprint in the Moldanubian Zone, Czech Republic: petrology, geochemistry and diffusion modelling of garnet zoning. Geol Rundsch 84:473–488

Owen JV, Dostal J (1996) Contrasting corona structures in mafic granulite from the Blanský Les complex, Bohemian Massif, Czech Republic. Can Mineral 34:959–966

Pan Y (1997) Zircon- and monazite-forming metamorphic reactions at Manitouwadge, Ontario. Can Mineral 35:105–118

Patchett PJ, Tatsumoto M (1980) A routine high-precision method for Lu–Hf isotope geochemistry and chronology. Contrib Mineral Petrol 75:263–267

Pettke T, Audétat A, Schaltegger U, Heinrich CA (2005) Magmatic-to-hydrothermal crystallization in the W-Sn mineralized Mole Granite (NSW, Ausralia), Part II: Evolving zircon and thorite trace element chemistry. Chem Geol 220:191–213

Roberts MP, Finger F (1997) Do U–Pb zircon ages from granulites reflect peak metamorphic conditions? Geology 25:319–322

Rubatto D (2002) Zircon trace element geochemistry: partitioning with garnet and the link between U–Pb ages and metamorphism. Chem Geol 184:123–138

Schaltegger U, Fanning CM, Günther D, Maurin JC, Schulmann K, Gebauer D (1999) Growth, annealing and recrystallization of zircon and preservation of monazite in high-grade metamorphism: conventional and in-situ U–Pb isotope, cathodoluminescence and microchemical evidence. Contrib Mineral Petrol 134:186–201

Scherer EE, Münker C, Mezger K (2001) Calibration of the Lu–Hf Clock. Science 293:683–687

Sun SS, McDonough WF (1989) Chemical and isotopic systematics of oceanic basalts: implication for mantle composition and processes. In: Sanders AD, Norry MJ (eds) Magmatism in the ocean basins. Geological Society Special Publication, London, pp 313–345

Svojtka M, Košler J, Venera Z (2002) Dating granulite-facies structures and the exhumation of lower crust in the Moldanubian Zone of the Bohemian Massif. Int J Earth Sci 91:373–385

Thirlwall MF, Walder AJ (1995) In situ hafnium isotope ratio analysis of zircon by inductively coupled plasma multiple collector mass spectrometry. Chem Geol 122:241–247

Thost DE, Hensen BJ, Motoyoshi Y (1991) 2-Stage decompression in garnet-bearing mafic granulites from Sostrene Island, Prydz Bay, East Antarctica. J Metamorph Geol 9(3):245–256

Tomaschek F, Kennedy A, Villa I, Lagos M, Ballhaus C (2003) Zircons from Syros, Cyclades, Greece—recrystallisation and mobilization of zircon during high pressure metamorphism. J Petrol 44(11):1977–2002

Tropper P, Konzett Y, Finger F (2005) Experimental constraints on the formation of high-P/high-T granulites in the Southern Bohemian Massif. Eur J Mineral 17(2):343–356

van Breemen O, Aftalion M, Bowes DR, Dudek A, Mísař Z, Povondra P, Vrána, S (1982) Geochronological studies of the Bohemian Massif, Czechoslovakia, and their significance in the evolution of Central Europe. Trans R Soc Edinb Earth Sci 73(for 1982):89–108

Vavra G, Gebauer D, Schmidt R, Compston W (1996) Multiple zircon growth and recrystallization during polyphase late Carboniferous to Triassic metamorphism in granulites of the Ivrea Zone (Southern Alps) an ion microprobe (SHRIMP) study. Contrib Mineral Petrol 122:337–358

Vavra G, Schmid R, Gebauer D (1999) Internal morphology, habit and U–Th–Pb microanalysis of amphibolite-to-granulite facies zircons: geochronology of the Ivrea Zone (Southern Alps). Contrib Mineral Petrol 134:380–404

Vrána S, Blümel P, Petrakasis K (1995) Metamorphic evolution. In: Dallmeyer RD, Franke W, Weber K (eds) Pre-permian geology of Central and Eastern Europe. Springer, Heidelberg, pp 453–466

Watson EB, Wark DA, Thomas JB (2006) Crystallization thermometers for zircon and rutile. Contrib Mineral Petrol 151:413–433

Wendt JI, Kröner A, Fiala J, Todt W (1994) U–Pb zircon and Sm–Nd dating of Moldanubian HP/HT granulites from south Bohemia, Czech Republic. J Geo Soc Lond 151:83–90

Whitehouse MJ, Platt JP (2003) Dating high-grade metamorphism constraints from rare-earth elements in zircon and garnet. Contrib Mineral Petrol 145:61–74

Wiedenbeck M, Alle P, Corfu F, Griffin WL, Meier M, Oberli F, von Quadt A, Roddick JC, Spiegel W (1995) Three natural zircon standards for U–Th–Pb, Lu–Hf, trace element and REE analyses. Geostand Newslett 19:1–23

Williams IS (1998) U–Th–Pb geochronology by ion microprobe. In: McKibben MA, Shanks WC III, Ridley WI (eds) Applications of microanalytical techniques to understanding mineralizing processes, vol 7. Rev Econ Geol, pp 1–35

Williams IS, Buick IS, Cartwright I (1996) An extended episode of early Mesoproterozoic metamorphic fluid flow in the Reynolds Range, central Australia. J Met Geol 14:29–47

Zack T, Moraes R, Kronz A (2004) Temperature dependence of Zr in rutile: empirical calibration of a rutile thermometer. Contrib Mineral Petrol 148:471–488

Zoubek V (1974) Remarques sur le Precambrien des zones mobiles de l'Europe Centrale et Occidentale. In: Zoubek V (ed) Precambrien des zones mobiles de l'Europe, Conf PICG, Liblice, Academia Prague, pp 33–62